International Journal of Clinical and Health Psychology 26 (2026) 100678

Contents lists available at ScienceDirect

International Journal of Clinical and Health Psychology

journal homepage: www.elsevier.com/locate/ijchp

Original article

Attention-based multi-feature fusion neuromarker for EEG-driven stress classification in learners

Saliha Ejaz [a], Soyiba Javed [a], Imran Shafi [a,b], Jamil Ahmad [b,c], Samuel Allende Monje [d,e,f], Josep Alemany-Iturriaga [d,g,h,i], Jin-Ghoo Choi [j], Imran Ashraf [j,*]

[a] Department of Computer and Software Engineering, College of Electrical and Mechanical Engineering, National University of Sciences and Technology (NUST), Islamabad 44000, Pakistan
[b] Department of Computing, Abasyn University, Islamabad Campus, Islamabad 44000, Pakistan
[c] Abdul Wali Khan University, Mardan 23200, Pakistan
[d] Universidad Europea del Atlantico., Isabel Torres 21, Santander 39011, Spain
[e] Universidade Internacional do Cuanza, Cuito, Bie, Angola
[f] Universidad de La Romana, La Romana, Dominican Republic
[g] Universidad Internacional Iberoamericana, Campeche 24560, Mexico
[h] Universidad Internacional Iberoamericana, Arecibo, Puerto Rico 00613, USA
[i] Fundacion Universitaria Internacional de Colombia, Bogota, Colombia
[j] School of Computer Science and Engineering, Yeungnam University, Gyeongsan 38541, Republic of Korea

ARTICLE INFO

Keywords:
Granger causality
Transfer entropy
Electroencephalography
Stress classification
Feature-fusion
Neuroscience

ABSTRACT

With the growing academic pressure and competitive educational environment, students often face mental stress, which can affect their academic performance and mental health. Its accurate and timely detection and prevention is important. Traditionally, mental stress has been reported by self-assessment, which is highly subjective and can be erroneous. With advances in neuroscience, electroencephalogram (EEG) signals have been used to study brain states more objectively. EEG-based features, including time-domain, frequency-domain, and various types of connectivity features, have been used to effectively classify stress signals. However, these individual features are only able to present one aspect of the brain under stress. Several studies have combined a distinct set of features extracted from EEG signals, including time and frequency domain features, with other peripheral signals. Stress is a complex mechanism which leads to alternation in brain dynamics, its connectivity patterns and information flow. This study proposed a feature-fusion model that can effectively combine spatial features, i.e. Microstates (MS), connectivity features like Transfer Entropy (TE) and Granger Causality (GC), which provided a new neuromarker for stress classification. These features are combined with attention fusion, which enhances the discriminant features and mitigates the individual limitations within each modality. We also extracted microstates for stress-based signals. It provided a new set of microstate topomaps to study brain networks when under stress, which was not explored previously. The proposed Attention-fusion based multi-feature set is classified using Support Vector Machine, Linear Discriminant Analysis (LDA) and Multilayer Perceptron (MLP) and gave a reliable accuracy of 95.47%, 98.91%, and 83.49%, respectively. To validate the proposed method, the classification results were compared with individual and binary fusion of MS, TE and GC features, which further confirmed the robustness of the framework. This proposed feature fusion provides a more robust stress classification neuromarker, which can effectively cover the brain dynamics for accurate reporting of the underlying mental state.

Introduction

Stress among students is increasing due to academic demands. High expectations for academic achievement and uncertainty about academic progress negatively affect the student's cognitive abilities. Its accurate and efficient identification of stress is important for maintaining students' academic performance and mental well-being. Without

* Corresponding author.
E-mail addresses: sejaz.cse23ceme@student.nust.edu.pk (S. Ejaz), soyiba.jawed@ceme.nust.edu.pk (S. Javed), imran.sha@abasyn.edu.pk (I. Shafi), jamil@ieee.org (J. Ahmad), samuel.allende@uneatlantico.es (S.A. Monje), josep.alemany@uneatlantico.es (J. Alemany-Iturriaga), jchoi@yu.ac.kr (J.-G. Choi), imranashraf@yu.ac.kr (I. Ashraf).

https://doi.org/10.1016/j.ijchp.2026.100678
Received 13 January 2026; Accepted 23 March 2026
Available online 1 April 2026

an effective coping mechanism and lead to long-term stress and other mental disorders. According to some reports, the number of students facing stress due to exam pressure and academic burden is increasing every year (Bouchrika, 2024). Stress is reported subjectively using traditional methods such as self-report and questionnaires. However, the subjective self-assessment is highly biased towards the reporting method, and emotional and behavioral states of the reporting person (Bolton et al., 2023). With the advancement in neuroscience and brain studies, scientists can study the complex brain networks using non-invasive techniques. Brain signals of various kinds reflect the activities of the central nervous system, providing a reliable way to studying the evoked functions (Chen et al., 2022). These signals have been used to classify various psychological conditions, such as emotion recognition, depression and motor imagery, including stress in students (Huckins et al., 2020). The early and reliable identification of stress can help provide personalized treatment and thus improve academic productivity.

Neuroimaging is a powerful field that helps understand the functions of the brain and the complex network using non-invasive techniques. Among the various techniques, Electroencephalography (EEG) stands out to be one of the sensitive method which captures the underlying electrical activity with high temporal resolution. This electrical activity is the result of postsynaptic potentials occurring in the cortical regions (Botvinik-Nezer & Wager, 2023). EEG has been a cutting-edge technique for studying neural responses because of its non-invasive nature. The brain operates under natural phenomena and can exhibit different properties when recorded through various representations. These different representations are typically known as Neuroimaging modalities. A few of them are EEG, functional Magnetic Resonance Imaging (fMRI), Positron Emission Tomography (PET), and Magnetoencephalography (MEG). These modalities capture distinct aspects of the brain. Due to its high temporal resolution, EEG-based signals have been used to study emotional and psychological conditions. It has various types of features that give information about underlying properties. The quantitative measure that contains information about signals and brain activity is called an EEG feature. There are various kinds of features that give distinct views about the neural activities. For example, Time-domain features in EEG give information about the temporal dynamics of the brain. Frequency-based features describe how varying brain activity produces a range of frequencies exhibiting distinct properties. Dynamic and static connectivity features give information about the network of the brain and its interaction with other regions.

The EEG features, when used standalone, give profound information about the nature of neuronal activities. It can help visualize brain performance when under various conditions, such as in rest, experiencing a strong mental task or under mental disorders. However, stress recognition remains a challenging task due to the complex dynamics of the brain. The simultaneous changes in its temporal, spectral and connectivity patterns are difficult to capture by the exact representation of the underlying phenomenon using any single feature or modality. These features fail to represent the holistic nature of complex brain dynamics and functioning when used individually. Therefore, it is essential to understand the relationships between these modalities. Multi-model fusion has emerged as a promising strategy to incorporate information from multiple modalities to improve accuracy (Chen et al., 2022). However, this fusion comes with challenges (Liu et al., 2023). One of these challenges is what features to fuse together to maximize the discrimination and variety of information. The answer to this depends upon the goal of fusion. So the appropriate selection of a limited yet discriminating set of features that also capture most of the brain changes is important. In recent studies, most fusion frameworks rely on redundant features, which do not consider effective interplay between linear, non-linear and temporal neural mechanics. Consequently, though a moderate level of performance is achieved, the underlying neural signatures for psychological disorders like stress are not fully understood.

Another issue is how to fuse these features. One of the issues regarding fusion is reported by Duan et al. (2024), i.e. dimension inconsistency. Different modalities can be fused at the feature-level (also known as early fusion) and decision level (also known as late fusion) (Zhang et al., 2020). The feature-level fusion accommodates heterogeneous feature sets but is followed by feature reduction, which leaves data sufficient for analysis. For decision-level fusion, a voting rule is applied to the final decisions produced by each modality.

To address these challenges, a fusion framework that aims to capture all the important aspects of the brain that are affected by stress is presented in this research. An attention-based fusion for Microstates is proposed, using Granger Causality and transfer entropy. The attention-fusion-based feature-level fusion method, instead of concatenating all features, selected appropriate features using attention. Among all the features, the attention-based model selects and assigns high weights to the most relevant and informative features. In this way, redundancy is reduced and only useful features from each modality set are forwarded. The rationale behind selecting these particularly distinct yet complementary characteristics is as follows:

- Microstates represent a quasi-stable brain image that provides temporal abstraction of the underlying cognitive process.
- Granger Causality quantifies the linear directed connectivity between signals. It is the measure of predictability from one signal to another. How stress modulates the connectivity is reflected in this study using Granger Causality.
- Transfer Entropy is a non-linear measure of directed information flow between signals, capturing important interdependences and information transfer during stress response.

Microstate analysis has been emerging as the latest way to study the resting-state dynamics of the brain. It has been used to analyze psychological disorders (S A et al., 2024; Terpou et al., 2022). However, Task-based Microstate extraction has not yet been explored by researchers. This study aims to derive a new set of data-driven Microstates that can provide temporal images of the brain when experiencing stress. This goal is supported by the fact that the dynamics of resting-state and task-based stress are distinct and provide distinct information. Therefore, a new way to explore Microstates for mental stress is proposed. By fusing heterogeneous features via an attention-based mechanism, this framework leverages the brain's temporal, linear, and non-linear aspects during stress, providing a more accurate representation of the brain.

The rest of the paper is structured as follows: Section "Literature review" provides an extensive overview of existing studies on Microstates, Granger Causality, Transfer Entropy and related features for psychological disorders classification, as well as fused features. The fusion model is explained in detail in Section "Methods", outlining the procedure adopted for data preprocessing. Feature extraction and classification architecture is explained in Section "Feature extraction". Section "Results and discussion" presents the evaluation results of the proposed methodology. To demonstrate the effectiveness of the proposed fusion model, an ablation study was carried out that compared the performance of individual feature sets for stress classification with that of fused features. Thereby validating the contribution of each component. Finally, Section "Conclusion" interprets the findings, their effectiveness and discusses the potential future works.

Literature review

Stress is a ubiquitous mental problem that affects people of every age and is faced especially by students worldwide. Stress is a psychological disorder that eventually leads to other mental and physical issues like depression (Aloufi, 2021), heart stroke and poor sleep (Pichandi et al., 2025). Academic stress faced by students often disturbs the functional patterns of the brain, leading to poor performance in academia

as well as draining mental health (Hag et al., 2021). It is important to prevent stress and its negative health outcomes (Malviya & Mal, 2022). The early detection of stress can prevent students from suffering from learning disabilities and adverse cognitive performance (Huckins et al., 2020).

There are many ways to report mental stress. Traditional methods involve self-assessment and reporting using questionnaires and other assessment tasks (Bolton et al., 2023). With advancements in neuroscience, scientists can use brain signals to study the brain and its complex regions using neuroimaging. These physiological signals are more objective and effective for better analyzing brain performance. A stressful situation produces the stress hormones that change bio-electrical signals. These fluctuations of electrical activity can be captured from the brain in the form of EEG signals. The EEG signals capture the electrical activity of neurons in the cortical region. EEG signals have high temporal resolution, which means that they can capture sensitive activities occurring in infinitesimally small time points. Stress is often released when a higher activity is experienced in the prefrontal cortex (Vignaud, 2023). The structural view also mentioned that the stress is produced by the left hemisphere of the brain Bhatnagar et al. (2023). Though it faces serious artifacts and many kinds of noise, EEG is a robust non-invasive technique that provides rich information about underlying activity and thus makes it suitable for real-time monitoring and analysis (Rashmi & Shantala, 2023).

EEG features

The brain signals need a quantitative measure to objectivize the reflected brain activity. These quantitative measures are called neuromarkers. They serve as an indicator of how the brain works. Neuromarkers identified from EEG signals are often derived from multiple feature domains such as time-based features, frequency features, time–frequency features, non-linear and connectivity features (Hu & Zhang, 2019). For instance, brain patterns are depicted in the form of multiple frequency bands, mainly Theta (4–8Hz), Alpha (8–13 Hz), Beta (13–30Hz) and gamma (30–100Hz), which are associated with different brain states. With the help of power distribution across these bands, scientists believe that stress is often related to increasing beta bands and lowering alpha bands (Bakare et al., 2024). Lokesh et al. quantified various frequency bands extracted from the physioNet dataset to classify stress and non-stress conditions and achieved an accuracy of 99.20% (Malviya & Mal, 2022). Similarly, using the power ratios between alpha, beta and theta bands, Rajendran et al. found that there is a rise in arousal index, cognitive attention and neural activity after performing stressful examinations (Rajendran et al., 2022). Another similar work for stress-based classification is done by Arsalan et al. (2019). Time–frequency features combine both time and frequency information of signals. The time–frequency features represented in 2-D spectrograms are also helpful to detect cognitive load, which corresponds to mental stress (Yedukondalu et al., 2024).

Connectivity EEG features

Stress increases cognitive performance, which results in non-linear and complex behavior of EEG signals. These non-linear behavior requires sensitive measures for their correct estimation. These measures, including Approximate Entropy, Lempel–Ziv Complexity and Higuchi's Fractal Dimension (HFD), are useful to study complex non-linear EEG signals (Javaid et al., 2024). For instance, (Cheng et al., 2019) used these features for neural remodeling of the brain and found that these non-linear features are helpful for functional recovery.

Stress is not produced in an isolated region of the brain; rather, complex emotions are produced by the communication between multiple regions, thus creating a network-level mechanism. Where traditional time and frequency domain features only collect the information from a localized region, they often fail to represent the interactions and communication of the vast brain network. During a complex brain activity, such as when multiple regions of the brain communicate and interact with each other, these connectivity patterns give important details about cognitive processes and sensory behaviors. The brain connectivity patterns can be studied in three distinct ways (Chiarion et al., 2023): *Structural connectivity* presents the anatomical pathways of information flow. *Functional Connectivity* gives the statistical relationship between brain regions. The *Effective Connectivity* describes the directional and causal link between multiple parts of the brain.

Functional connectivity is defined as the statistical interdependence of spatially distant neuronal regions, usually measured by Pearson's correlation, coherence and Phase Locking Value PLV (Cao et al., 2022). Higher values of correlation represent a more robust relationship between the corresponding EEG signals. For the task of motor-imagery classification, the dynamic functional connectivity of the brain extracted from a shorter interval of time is used and achieves the accuracy of 85.5% (Shamsi et al., 2021). A study proposed an interesting methodology in which a person's mental workload level is analyzed using functional connectivity analysis of obtained Microstates, with graph-theory-based analysis for each frequency band. The authors were able to achieve an accuracy of 95.3% (Yedukondalu et al., 2024). Instead of classifying the signals directly based on PLV values based on functional connectivity matrices, authors of Zhang et al. (2023) developed a set of new distance-based matrices to combine statistical and frequency domain information. The highest accuracy among these distance metrics was obtained to be 84% for the delta band, 83.96% for the alpha and 83.56% for the beta band for the task of emotional recognition. But these simpler methods come with limitations. Pearson's correlation value only captures the linear link.

Stress-based EEG signals require a more nonlinear approach that considers mutual information and direct interdependencies between two or more brain regions. Although cross-correlation functions have been effective in studying undirected interaction, both correlation and mutual information lose temporal dependencies of a signal as they measure the connectivity irrespective of the time the signal occurred. Effective connectivity analysis indicates the causal or directive link between these regions, which is not captured by functional connectivity. And these directive links and mutual information sharing are effective for classification. For example, a study extracted various kinds of features, including Phase-locking value, Permutation Entropy, Mutual Information and Spectral Entropy, and found that the highest discriminative results were given by Mutual Information MI and Entropy (Goenka et al., 2022). One study found that information transfer is greater in the alpha band when eyes are closed than when eyes are open (Restrepo et al., 2023). Electromagnetic Source-Imaging ESI estimates the neural activity from the surface of the brain. The authors of Sohrabpour et al. (2016) are convinced that combining ESI with directed Granger Causality reduced the effect of volume conduction that effectively determines the brain regions involved in Motor Imagery. The research accounts for information transfer in inter-hemispheric regions using transfer entropy.

Methods like Granger Causality are used to assess how the past values of a signal can predict the future values of another signal. Granger Causality considers that the signals are stationary. Many useful algorithms have been proposed to handle the issue of non-stationarity in EEG signals. For example, Zhang et al. used time-varying directed network spectrum obtained from causal links using Granger Causality (Yi et al., 2024).

Similar to Granger Causality, a model-free method to find the directed links between signals is transfer entropy. It is based on delayed interaction between a cause (predicting signal) and effect (predicted signal) using information theory. It captures non-linear forms which are overlooked by linear approaches like Granger Causality (Bastos & Schoffelen, 2015). An effective study was conducted by Gao Z. et al. in which Transfer Entropy was used to find the directed link between EEG and EMG for motor-cortex imagery (Guo et al., 2022). With the help of information transfer, Transfer entropy is used to see the regulatory patterns introduced by medication on Parkinson's diseases (Zhu et al.,

2025). Another study which combined Transfer Entropy and Granger Causality with their respective Histogram of Oriented Gradients (HOG) images. HOG is the graphical representation of channel-to-channel connectivity. A vast amount of gradient-based features are present in this graphical image. The authors of Gao et al. (2020) combined Transfer Entropy and Granger Causality with its HOG and observed about 12% of classification accuracy improvement. However, no fusion of the two modalities was made to see their combined effect.

Spatial features

Spatial configuration of brain activity is also helpful to keep track of neural activities over time. Spatial Microstates give unique configuration of brain topomaps which remain stable for a brief period of time. The temporal evolution of instantaneous scalp potential topography gives a long-range connectivity pattern of a network. Recently, researchers have been using Microstate patterns as a tool to diagnose chronic cognitive diseases (Li et al., 2023). Microstates are small quasi-stable states of the brain which give dense information about spatial organization, temporal dynamics and patterns that change after an external stimulus. Microstates, first proposed by Lehmann et al. is an interesting property that says that significant information of entire temporal patterns could be represented by a few maps (Koenig et al., 2024). Initially, Microstate analysis was carried out in the resting state only. Canonical microstates, often labeled A, B, C, and D, represent stable patterns commonly identified in resting-state EEG and are thought to correspond to fundamental cognitive and sensory networks. However, recent studies have used Microstates for the rapid detection of brain disorders (S A et al., 2024). One study extracted about 5 Microstates from resting-state EEG signals of major depressive disorder MDD signals (Li et al., 2023). Based on classification, the authors can analyze the temporal patterns of Microstates in depression by achieving an accuracy of 89.09%. Also, a varying number of Microstates extracted from resting state signals corresponds directly to the Resting State Network RSN of the brain Michel and Koenig (2018). Microstates, along with drug concentration response towards behavioral consciousness, also played an important role in studying the alterations in conscious state after taking anaesthesia (Liu et al., 2022).

Most of the existing studies rely on pre-defined canonical states (Haydock et al., 2025). The data-driven Microstates extend the use of microstates to detect adaptability to individual- and task-based variability (Han et al., 2025). It has allowed us to identify and study specific cognitive impairment like Attention-Deficit Hyperactivity Disorder (ADHD) through specific syntax of Microstates (Alves et al., 2022).

An attempt was made to classify task and resting-state signals based on Microstates (Kim et al., 2021). The authors extracted Microstates from task-based and resting state signals. About four canonical states were extracted from each type of signal. On the basis of extracted time-based features such as occurrence and mean duration, the highest area under the curve on receiver operating curve (ROC) plot was achieved with a value of 0.831. Microstates extracted from frequency bands also reflect comparable results. One study investigates that motor imagery tasks show a prominent influence on Microstates extracted from the alpha band Xiong et al. (2025). Similarly, the alpha band also showed the classification results of 76% for the classification of Microstate-based post-traumatic stress disorder (Terpou et al., 2022).

Feature-fusion

Despite the extensive work done on accurate feature fusion of multiple EEG features, a primary limitation is the lack of comprehensive fusion of between modalities. A joint neural feature set for emotion recognition was revealed by studying EEG based Microstates temporal features and FNIRS based spatial patterns leveraging multimodal feature for effective neuromarkers (Si et al., 2024). But this method does not explicitly fused both feature sets. While Microstates inherently capture spatio-temporal features, their integration with other time-domain, frequency-domain and various kinds of connectivity features remains unexplored. Another critical gap is the extraction of stress-based data-driven Microstates. This gap is supported by the fact that brain dynamics change to a greater extent when under any heavy mental workload, as compared to the resting state brain network.

Recently, a technique named Deep Canonical Correlation (DCC) has been used to integrate features from multiple modalities such as EEG and eye movement (Qiu et al., 2018). This technique combines the features into a unified space and maximizes the correlation to perform feature-level fusion. CNN and self-attention are used by Ma et al. (2024) to encapsulate the temporal information from multi-model EEG signals, along with covering the global dependencies between them extracted. The limitation in existing studies shows that single-domain features might not fully capture the multifaceted nature of physiological responses. Several studies are focused on using only a limited number of features from multiple sets after combining them (Swapnil et al., 2024). For example, the authors of Hag et al. (2021) are convinced that fusing time, spectral and connectivity-based features can perform better in classifying stress vs relax states. The features extracted from time domain features, such as kurtosis, skewness, peak-to-peak amplitude, Hjorth, frequency features extracted from frequency bands and connectivity features extracted using phase-locking value, give a total of 210 features, from which only optimum multi-domain features (a total of 68) were used for classification. Another multi-model fusion model is developed by Chen et al. (2022) for fusing EEG signals with other peripheral physiological signals PPS such as EMG, and proved that multi-model fusion gives significant performance improvements in classifying stress based on valence and arousal.

EEG features have also been combined with other physiological signals, such as the Electrocardiogram (ECG) signals. The proposed solution effectively fused time series of both modalities on the basis of time–frequency ridge mapping (Bahador et al., 2021). Another unique approach uses the Granger Causality connectivity pattern to quantify the causal configurations between EEG channels using transfer entropy (Ramakrishna et al., 2021). The authors developed an emotional recognition method using this Granger Causality-Transfer Entropy-based method and achieved an accuracy of about 90%.

Structural and functional features have inconsistent feature dimensions. It is important to fuse them in a way that no information is lost. To address this problem, an effective method for feature combining and selection is proposed by Yang et al. (2018). The structural patterns are constructed from the cortical and subcortical regions of interest. Similarly, the functional connectivity matrix is extracted using Pearson's correlation coefficient between the mean time courses of each pair of Regions of Interest (ROIs). The feature reduction framework preserves inter-modality relationships and achieves an accuracy of 84.91%.

A hybrid pool of features collected from the time domain and wavelet-based bandwidth-specific features is used for classification (Hasan & Kim, 2019). A framework that ranks the features on the basis of relevance instead of considering the entire pool is proposed. The fusion improved the accuracy up to 73.38%. Akhand et al. improved the accuracy of emotion recognition by fusing Connectivity Feature Maps (CFMs) from multiple features, such as Pearson Correlation Coefficient (PCC), Mutual Information (MI), Transfer Entropy and Phase-Locking Value (PLV) using Convolutional Neural Network (CNN) and found that a fused set of CFMs gives better results. Among all binary fusions, PVL and MI give the highest accuracy of 90.71% for valence and 91.15% for arousal. The feature-level fusion is performed by fusing the upper and lower triangles of the CFM's matrix.

The existing literature suggests that single-modal features are often insufficient, and integrating them can lead to significant improvements in classification (Pillalamarri & Shanmugam, 2025). The transition from single-feature analysis to multimodal feature fusion marks a crucial advancement in developing highly accurate and reliable EEG-based stress classification systems. Table Table 1 gives a detailed comparison between multiple feature extraction studies.

Table 1
Literature review for feature fusion techniques for EEG based signal classification.

Ref	Domain	Features	Classifier	Task	Accuracy
Hag et al. (2021)	Time-domain	Kurtosis, skewness, peak-to-peak amplitude, Hjorth	SVM	Stress	81.4%
	Frequency-Domain	Delta, theta, alpha, sigma, beta			80%
	Connectivity	PLV			88%
	Fusion	Feature-Level Fusion			93.3%
Chen et al. (2022)	EEG	Channel-level time-space and frequency-space graph sequence.	Attention Recurrent Graph Convolutional Network	Emotion Recognition	87.61%
	Peripheral physiological signals				–
	Fusion	Data-Level Fusion			92.50%
Yang et al. (2018)	Structural Features	Cortical ROIs	Hierarchical feature reduction	Major depression	81.4%
	Functional Features	PLV			–
	Fusion	Feature-Level Fusion			84.91%
Gao et al. (2020)	Granger Causality	Linear network features	SVM	Emotion Recognition	73.18%
	Granger Causality + HOG	Linear + gradient features			88.93%
	Transfer Entropy	Non-linear network features			81.88%
	Transfer Entropy + HOG	Non-linear +gradient features			95.2%
Hasan and Kim (2019)	Time-domain	Root mean square, kurtosis, skewness, shape factor, etc	PCA + KNN	Stress Classification	69.26%
	Frequency-Domain	Level 5 discrete wavelet transform (DWPT)			
	Fusion	Feature-Level Fusion	Feature selector + KNN		73.38%
Zhang et al. (2022)	Time series	–	Decision Forest	Depression Recognition	78.33%
	Spatial Visibility Graph	–			72.97%
	Fusion	Feature-Level Fusion			90.60%
Bahador et al. (2021)	EEG + ECG	Time-frequency Fusion	RNN	monitoring the depth of Anesthesia	90.37%
Chen et al. (2015)	EEG + PERI Fusion	Decision-level Fusion	HMMs	Emotion Recognition	75.63%
		Feature-level Fusion			85.63%
Akhand et al. (2023)	Connectivity Features	PCC	CNN	Emotion Recognition	(88.22%) Arousal (87.43%) Valence
		MI			(90.14%) Arousal (89.98%) Valence
		TE			(73.65%) Arousal (73.22%) Valence
		Phase-Locking Value PVL			(88.22%) Arousal (87.63%) Valence
		PCC + MI			(90.43%) Arousal (89.71%) Valence
		PCC+ TE			(86.43%) Arousal (86.16%) Valence
		PLV + MI			(91.15%) Arousal (90.71%) Valence
		PLV+TE			(85.84%) Arousal (85.57%) Valence
		MI+TE			(90.68%) Arousal (90.12%) Valence
Radman et al. (2021)	Temporal	Root Mean Square, Variance, Mean Absolute Value Kurtosis, Skewness.	Ensemble Decision Tree (EDT) Classifier	Seizure Detection	–
	Spectral	Power Spectral Ratio, Skewness, BP, Variance, Median Power Frequency.			–
	Fusion	Feature-Level			99.33%

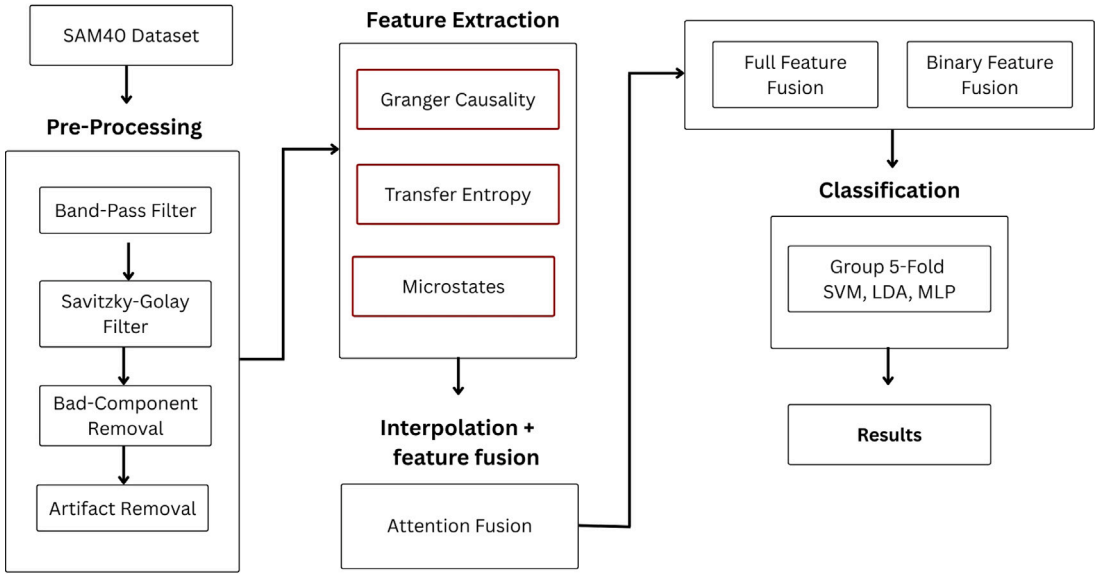

Fig. 1. Block diagram of proposed framework for stress detection.

Research gaps and research objectives

- Most of the existing studies on Microstates focus on the resting state of the brain. Stress activates the cortical region of the brain and which gives rise to spatiotemporal dynamics which are different from the resting state. Therefore, analyzing stress-related Microstates on the basis of pre-defined canonical Microstates fails to uniquely capture stress-related configurations.
- Although the existing studies mostly combine time, time–frequency and other types of connectivity features, Microstates features capture global temporal network organization, offering complementary information. No, studies up till now have fused Microstates with any other modality.
- Prior studies either combined linear or non-linear connectivity features in isolation. However, the brain is composed of many linear as well as non-linear interdependencies, as well as dynamics captured by Microstates. No existing study has utilized the combined effect of linear Granger Causality features, non-linear directed features and temporal network features for stress classification.

To resolve the identified research gaps, the following research objectives are proposed:

- **Research Objective 1:** Develop characterized stress-specific Microstates based on a data-driven clustering technique. These Microstates will be analyzed on temporal parameters such as duration, occurrence, probability of transition and coverage.
- **Research Objective 2:** Develop a multi-model fusion model that evaluates the impact of Microstate inclusion on improving the classification of stress-based signals.
- **Research Objective 3:** Develop a model that analyzes the impact of the complementary nature of distinct features on stress detection.

Methods

Early identification of stress patterns can aid in the development of preventive strategies, improve mental health monitoring, and thus help students perform efficiently in academics. Here, a novel multimodal fusion framework is proposed that integrates three complementary EEG analysis techniques i.e. Microstate Analysis, Transfer Entropy, and Granger Causality which helps to capture the most effective and discriminating dynamics across all three modalities and thus efficiently classify the signal.

For the study, three important feature sets are discussed: Granger Causality, Transfer Entropy TE and Microstates . Microstates provides vast information about the spatial and temporal changes that occur in the brain network using only a few distinct topomaps. Transfer Entropy and Granger Causality are both measure of effective connectivity that gives information about causal links between different brain regions. Granger Causality is a parametric method which explains whether a signal emerging from one part of the brain can help predict the future values of other brain regions. Granger Causality is a linear method which tries to deal with stationary signals. Transfer Entropy is a non-parametric model-free measure of information transfer, which is suitable for non-linear signals as stress. All three feature sets provide enriched information about the brain's temporal information, information transfer and causal interactions that are important for discriminating stress and relax states. Fig. 1 depicts the detailed view of the proposed methodology.

The SAM40 (Ghosh et al., 2022) dataset is selected to build the stress neuromarker. SAM40 provides a high-quality EEG signal recorded from an equal number of both stress and relax signals. There is a variety of stressors introduced in research, but for this study, the stress signal generated from mental arithmetic tasks is taken into consideration, as mental mathematical tasks increase activity in the prefrontal cortex, which results in cognitive load and performance anxiety. This dataset is a collection of EEG recordings of 40 individuals (14 female and 26 male students) with an average age of 21.5 years, which offers appropriate robust model training and evaluation while maintaining generalizability across individuals. The data is recorded from the 32-channel Emotiv EPOC kit with a sampling frequency of 128 Hz. Each subject has two separate recordings, i.e. for the stress and relax state. The raw form of each signal is in matrix form of 32x3200, where 3200 are the time points.

Before processing, the dataset is carefully preprocessed to remove any kind of noise which might affect the final results. For that, raw data is first filtered to remove most of the physiological and non-physiological artifacts. The Savitzky–Golay filter is used for re-referencing. This filter helps remove noise and smoothens the signals. Unlike other moving-average filters that blur out peaks, Savitzky–

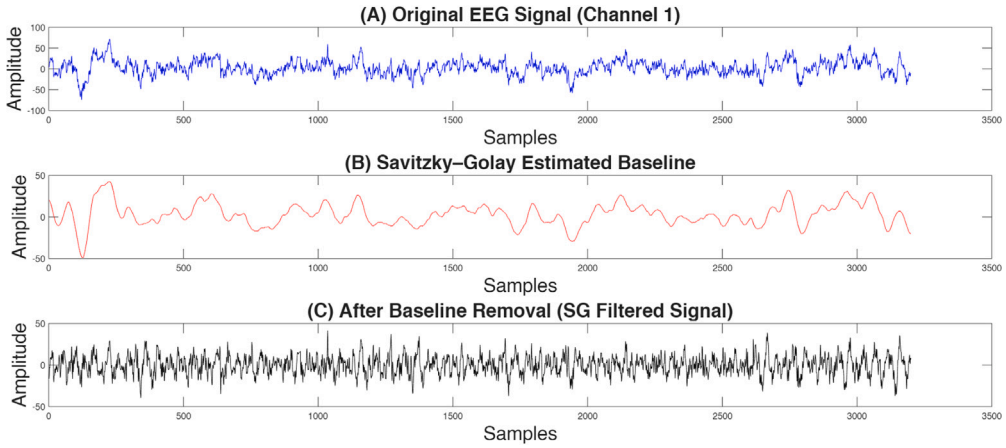

Fig. 2. Savitzky–Golay filtering process. (A) is the original signal from channel 1 for subject 10. (B) shows the averaging trend that is provided by Savitzky–Golay filter. This averaging trend (B) is subtracted from original signal (A) and resulted in the smooth shown in (C).

Golay filters preserve higher-order signal characteristics, such as sharp transitions that are most likely to occur in stress signals. For an input EEG signal $x(t)$, the SG-filtered output $\hat{x}(t)$ can be expressed as:

$$\hat{x}(t) = \sum_{i=-k}^{k} c_i \, x(t+i) \tag{1}$$

where c_i are the polynomial coefficients determined through least-squares fitting. The baseline-corrected signal is then obtained by subtracting the estimated trend:

$$y(t) = x(t) - \hat{x}(t) \tag{2}$$

The window length is kept at 127, and the polynomial order is 5. The SG filter subtracts the slow drifts and results in a smooth signal. Fig. 2 shows the sample EEG signal in its raw form (A), and (B) is the $\hat{x}(t)$ smoothing trend. Finally, the (C) figure shows the averaged signal after removing the baseline. To remove the high-frequency, the Discrete Wavelet Transform DWT filter is used. The DWT decomposes the signals into approximation, using a High-pass Filter HPF and detailed components, using a Low-pass Filter LPF. The db2 filter decomposes the signal into 4-levels sub-bands namely A4(0–4Hz), D4(4–8Hz), D3(8–16Hz), D2(16–32Hz) and D1(32–64Hz). Fig. 3 shows the detailed and approximation coefficients for a signal. This filtering typically removes the noise and frequency above 64 Hz.

Finally, EEGLAB is used to remove bad channels and components after applying Independent Component Analysis ICA. The typically removed artifacts were lateral eye movement and eye blinking artifacts.

Feature extraction

In this section, feature extraction was performed to capture distinct neural dynamics from EEG signals using three complementary approaches: Granger Causality, Microstate Analysis, and Transfer Entropy. These techniques collectively quantify directional connectivity, temporal stability of brain states, and information flow between channels, providing a comprehensive representation of the brain's functional organization.

Granger causality

Different parts of the brain work in harmony with each other to perform any specific task. The neuronal connections can sometimes superimpose to generate a signal or sometimes inhibit each other. Granger proposed that if past values of a certain signal predict the future values of another signal, then there exists a causal link between these two. The same principle is applied here to signals originating from different parts of the brain. By applying the Granger phenomenon on brain signals, it can be predicted if causality exists in different cortical regions during mental tasks like stress.

Granger Causality is more of a predictive idea of how one signal is "causing" the future value of another signal using statistical measures. Grange Weiner is convinced that if there are two time signals $X(t)$ and $Y(t)$, then the previous value of X, i.e. $X(t-i)$ and of Y, i.e. $Y(t-i)$, can predict the future value of Y, i.e. $Y(t+1)$. If the prediction is found to be similar, then it is said that Y contain some information about X. This relationship between X and Y is not straightforward. This is because the brain signals are often influenced by neighboring signal channels and by other parts of the brain. Using an unrestrictive autoregressive model, the Granger Causal link between $X(t)$ and $Y(t)$ can be presented by:

$$Y(t) = \sum_{i=0}^{p} a_i X(t-i) + \sum_{j=0}^{q} b_j Y(t-j) + \varepsilon_{Y|X^*,Y} \tag{3}$$

A causal link is the linear weighted combination of previous time points. Where a_n and b_n are autoregressive model coefficients and GC $= \ln\left(\varepsilon_{Y|X^*,Y}\right)$ is the residual error or variance of the signal. For $GC = \ln\left(\frac{\varepsilon_{Y|Y^*,Y}}{\varepsilon_{Y|X^*,Y}}\right)$, if $GC < 0$ then there is no causal link between X and Y. The causal link exists when the GC value is above 0.

The Vector Autoregressive model (VAR), differs from the Dynamic Causal Modelling (DCM) technique in that DCM relies on pre-specified brain mechanisms for how neurons interact. VAR is independent and generic, and it does not rely on how brain data is captured (Barnett & Seth, 2014). Also, a VAR is efficient in estimating many non-linear processes. The bivariate autoregressive (unconditional) model has limitations when applied to EEG signals from multiple channels. As a signal coming from one channel may be the superposition of information coming from multiple channels. In that case, a multivariate autoregressive (conditional) model will be used. A conditional GC-based method computes the predictive link between two channels while accounting for information from other channels. In the SAM40 dataset, each signal has dimensions of 32 × 3200 (channels × time points). For calculating the causal link of each channel, a multivariate model will be constructed.

$$\begin{pmatrix} X_1(t) \\ \vdots \\ X_{32}(t) \end{pmatrix} = \sum_{n=1}^{p} a_n \begin{pmatrix} X_1(t-n) \\ \vdots \\ X_{32}(t-n) \end{pmatrix} + \begin{pmatrix} \varepsilon_1(t) \\ \vdots \\ \varepsilon_{32}(t) \end{pmatrix} \tag{4}$$

Stationarity and stability

In the case of an EEG signal, the pattern of synchronization changes the temporal dynamics of the signal to a greater extent. Also, Granger Causality works best with a stationary and stable signal (Barnett &

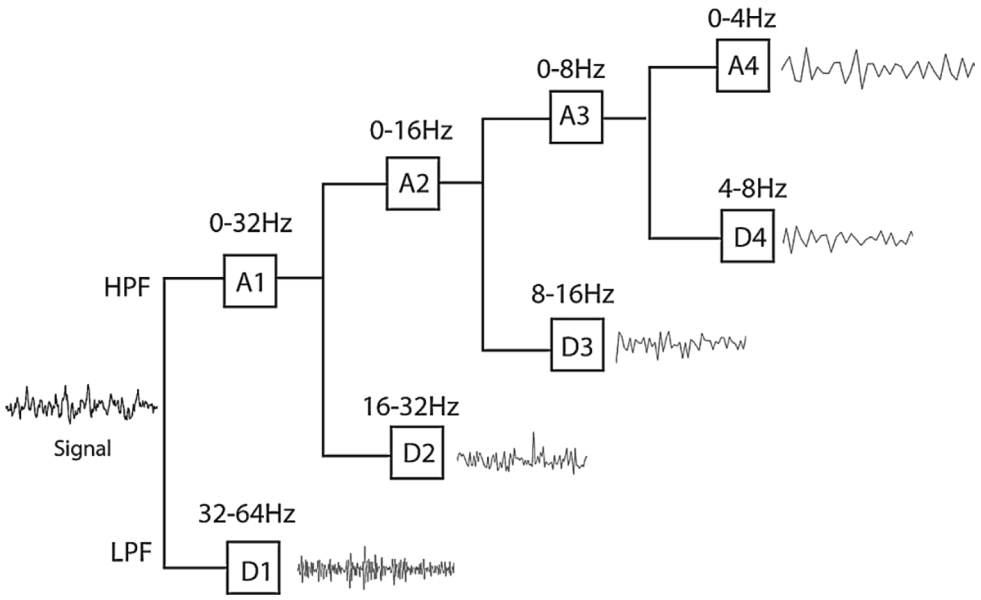

Fig. 3. 4-level discrete wavelet transform (db2) filter decomposition.

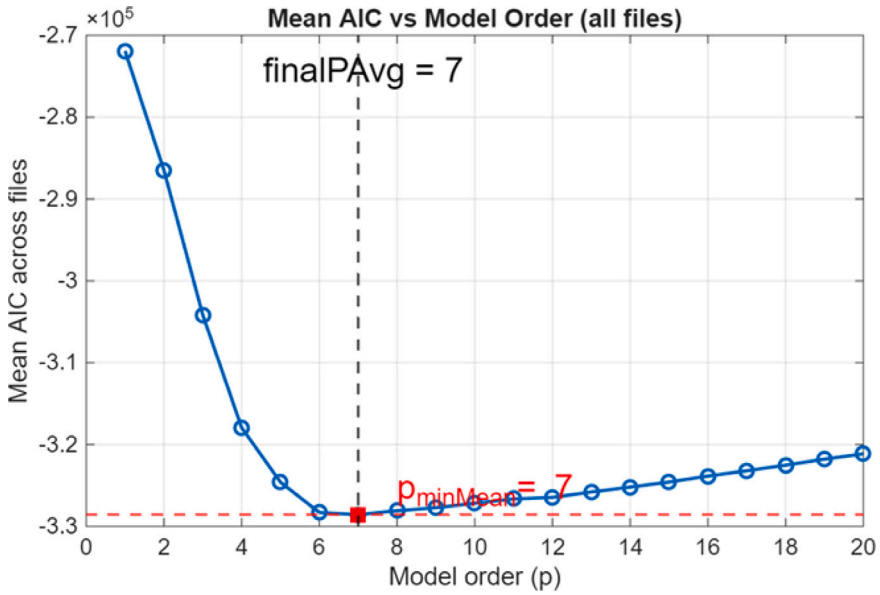

Fig. 4. Value of AIC against the model order P. The value of P ranges from 0 to 20. For each p, AIC is calculated across all signals (files). The smallest value of AIC is given by P = 7, indicating the least squared errors for model parameters.

Seth, 2014). For stationary signals, the statistical features such as mean, variance remain constant over time. For task-based EEG signals, such as in the case of mental assessment tasks, the signals are absolutely non-stationary. Granger Causality is applied to see the linear connection between EEG signals. Granger Causality requires the signal to be stable as well. By stability of a system means that a finite input does not give infinite output, or in other words, does not "blow up" the system. Using MATLAB's Var-spectral function, the unit complex z-plane value is obtained to be 0.91, i.e. less than 1, indicating that the signals are stable. In the context of VAR, if the multivariate VAR coefficient a_n is stable, then the signal is said to be stable. For a_n, it is stable if it lies within the unit complex z-plane.

$$\det(\phi(z)) = I_n - a_1 z^1 - a_2 z^2 - \cdots - a_{32} z^{32} > 1 \quad (5)$$

The MVGC built-in function, *var_specrad*, automatically finds if a_n is stable or not.

Model parameter estimation

The model order is the number of time points considered for modeling. The higher order number increases the complexity of the model but provides more sensitive information there, whereas for a lower order value, the model becomes simpler but less dependent on the previous history of the signal. Akaike Information Criterion (AIC), Bayesian Information Criterion (BIC) and Hannan-Quinn Criterion (HQ) are important and useful methods which are considered in the literature for model order estimation (Placek et al., 2022). For model order estimation, a multivariate AIC for the VAR value will be used here. AIC value is calculated for each signal and then averaged across all signals for each value of p. The value of p with the minimum sum of squared errors is selected as the model parameter. Fig. 4 shows the AIC value of all subjects averaged over a range of p from 2-20. The lower Ordinary Least Squares value is obtained for p = 7 (indicated by the red line in Fig. 4). After applying the proposed setup, the outcome of the G-causal.

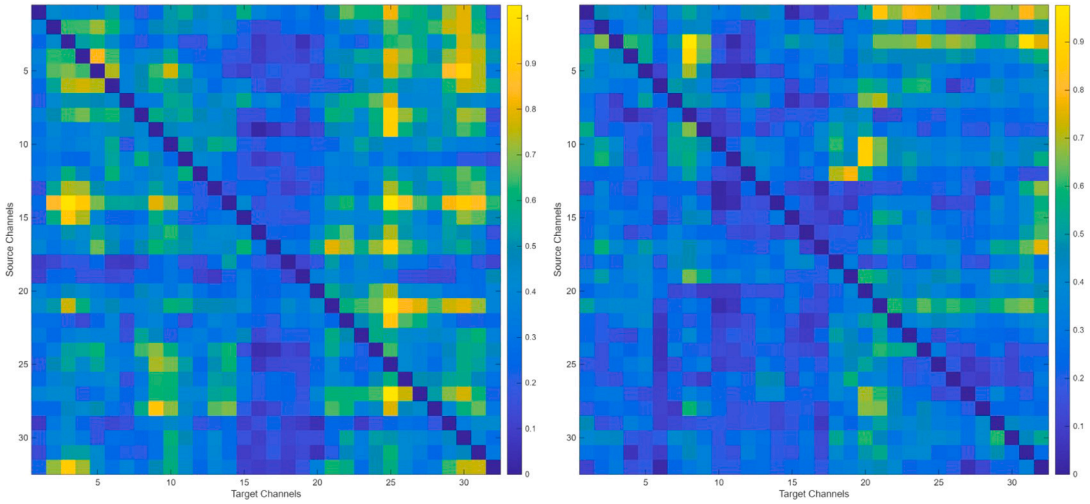

Fig. 5. The Granger causal link between 32 channels signals for subject 10. Stress (left) and relax (right). The source channels are presented on the vertical axis, and the target channels are presented in horizontal axis.

$$\mathrm{AIC} = T \ln\left(\det(\Sigma_p)\right) + 2p \tag{6}$$

where T is the number of time points, $\Sigma_p = \mathrm{cov}(\epsilon_t)$ is the residual variance matrix of the current order of the AR model (P). AIC is based on maximum likelihood estimation and selects the best fit where the variance $(\det(\sum p))$ is minimum. AIG is calculated for each signal for a range of values of p and averaged across all signals. The optimal AIG with the minimum value of the Ordinary Least Squares (OLS) method, which minimizes the sum of squared errors of VAR coefficients.

$$Y = AZ + E \tag{7}$$

Y is the predicting variable, and A is the multivariate VAR coefficient $n \times np$, where n is the number of individual channels.

$$\Sigma_p = \frac{1}{T-p} EE^T \tag{8}$$

For 32 channels C=1,2,3, ….32, and $X_{(t)}$ is a time series, the Granger Causality link between the source s and destination d, is based upon the residual variance produced by the past value of d $\varepsilon_{d|d^*,d}$ as well as on the variance of the past values of all other conditioning sources s, $\varepsilon_{d|d^*,\{C\}}$, where $S = C \setminus \{i\}$. In other words, it can be stated that when a certain time series Granger causes another time series, it is based upon the residual variance of two regressive models, i.e. the full restrictive model $\varepsilon_{d|d^*,d}$ and reduced non-restrictive models $\varepsilon_{d|d^*,\{C\}}$. The Granger pair value is evaluated based on the residual variance between each channel.

$$\mathrm{GC}_{i\to d|\{C\}} = \ln\left(\frac{\varepsilon_{d|d^*}}{\varepsilon_{d|d^*,\{C\}}}\right) \tag{9}$$

The Granger Causality (Fig. 5) quantifies the directional influence between EEG channels, revealing causal interactions and connectivity patterns within the brain. While Granger Causality effectively captures linear dependencies, it may overlook nonlinear interactions that are often present in neural dynamics. To address this limitation, Transfer Entropy is applied as a nonlinear and model-free measure of information flow between EEG signals, providing a deeper understanding of dynamic causal relationships beyond the assumptions of linearity.

Stationarity and stability

In the case of an EEG signal, the pattern of synchronization changes the temporal dynamics of the signal to a greater extent. Also, Granger Causality works best with a stationary and stable signal (Barnett & Seth, 2014). For stationary signals, the statistical features such as mean, variance remain constant over time. For task-based EEG signals, such as in the case of mental assessment tasks, the signals are absolutely non-stationary. Granger Causality is applied to see the linear connection between EEG signals. Granger Causality requires the signal to be stable as well. By stability of a system means that a finite input does not give infinite output, or in other words, does not "blow up" the system. Using MATLAB's Var-spectral function, the unit complex z-plane value is obtained to be 0.91, i.e. less than 1, indicating that the signals are stable. In the context of VAR, if the multivariate VAR coefficient a_n is stable, then the signal is said to be stable. For a_n, it is stable if it lies within the unit complex z-plane.

$$\det(\phi(z)) = I_n - a_1 z^1 - a_2 z^2 - \cdots - a_{32} z^{32} > 1 \tag{10}$$

The MVGC built-in function, *var_specrad*, automatically finds if a_n is stable or not.

Transfer entropy

Transfer entropy is a measure of directional information transfer between two entities based on information theory. Transfer Entropy is useful in the sense that it can capture the asymmetric and nonlinear dependencies between signals. In neuroscience, Transfer Entropy can help us to know how information is transferred between multiple sources of signals. The purpose of using TE here is to see if the uncertainty measure of information transfer between multiple brain regions can be effective for the classification of different brain states, such as stress and relax.

TE helps find the information transferred between brain regions. Since the TE considers this communication without assuming a specific relationship between signals; it is more applicable to nonlinear systems. Transfer entropy (Sadeghijam et al., 2021), tells about how much the past values of $X(t)$ reduce the uncertainty of future values of another signal $Y(t)$ given $Y(t)$'s own past values in Eq. (11).

$$H(X \mid Y) = H(X,Y) - H(Y) \tag{11}$$

If there is a directed causal link and information flows from X to Y, then the transfer entropy TE from X to Y is the information flow from both $Y(k)$ and $X(k)$ mutually minus the information received from $Y(k)$. Expanding the conditional entropy in terms of joint entropy in Eq. (12).

$$T_{X\to Y} = H(Y_{t+1}, Y_t^{(k)}) + H(Y_t^{(k)}, X_t^{(l)}) - H(Y_t^{(k)}) - H(Y_{t+1}, Y_t^{(k)}, X_t^{(l)}) \tag{12}$$

In terms of joint entropies, the Transfer Entropy from X to Y is defined as the uncertainty between Y's future and its own past values,

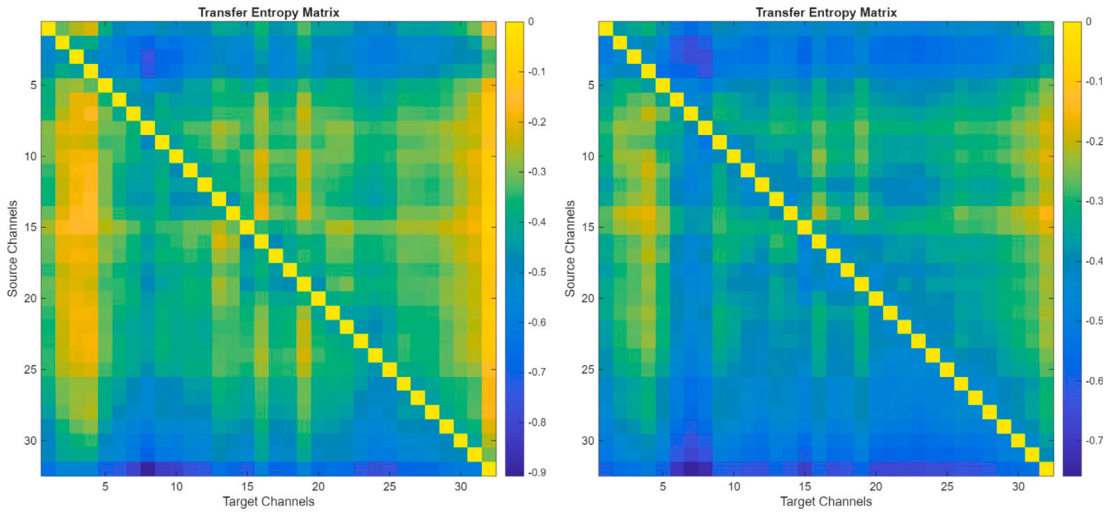

Fig. 6. Transfer entropy values between 32 channels signals for subject 10. Stress (left) and relax (right). The source channels are presented on the vertical axis, and the target channels are presented on the horizontal axis.

$H(Y_{t+1}, Y_t^{(k)})$, combined with the uncertainty of the past of both signals, $H(Y_t^{(k)}, X_t^{(l)})$, excluding the joint uncertainty of the complete system, $H(Y_{t+1}, Y_t^{(k)}, X_t^{(l)})$, and Y's own uncertainty, $H(Y_t^{(k)})$. There are multiple methods to estimate transfer entropy. This framework assumed that the underlying processes are approximated by a Gaussian assumption. The differential entropy of Gaussian Z with variance σ^2 is given by:

$$H(Z) = \frac{1}{2}\log\left(2\pi e\,\sigma^2\right) \tag{13}$$

Applying the Gaussian entropy on predictive signals, Y_{t+1} given its own past values, the entropy is $H(Y_{t+1} \mid Y_t)$

$$H(Y_{t+1} \mid Y_t) = \frac{1}{2}\log\left(2\pi e\,\mathrm{var}(Y_{t+1} - Y_t)\right) \tag{14}$$

The conditional entropy of Y_{t+1} given both its own past and the X's past X_t is expressed as:

$$H(Y_{t+1} \mid Y_t, X_t) = \frac{1}{2}\log\left(2\pi e\,\mathrm{var}(Y_{t+1} - (Y_t + X_t))\right) \tag{15}$$

Microstates analysis

The Microstates can be defined as a stable set of brain patterns that usually last for about 60–120ms before transitioning into a new stable state. At rest, the brain experiences a distinct functional state for a certain amount of time (Fig. 6). Researchers believe that a set of a few of these functional states can help explain most of brain analysis. The Microstates are often referred to as "atoms of thoughts" due to their repeating patterns and stability across time signals. The idea of Microstates comes from resting state brain analysis, when it was believed that the brain remains inactive during rest until some external stimuli activate the brain Michel and Koenig (2018), where it is found that resting state Microstates analysis of the brain can reflect multiple neuropsychiatric diseases (Khanna et al., 2015; Li et al., 2023). However, few functional brain states can be helpful to explain Microstates are used to explore the intrinsic properties of temporal correlation of neuronal regions during resting states.

Global field potential

Global Field Potential (GFP) is the measure of the relative potential difference between an instantaneous potential $V_n i(t)$ and the mean potential across all channels $V_n(t)$. The GFP can be calculated using Eq. (16) where N is the number of channels. The GFP time series is subjected to a peak detection procedure to identify local maxima, which correspond to moments of maximal global neuronal synchronization and represent stable scalp potential topographies.

$$\mathrm{GFP}(t) = \sqrt{\frac{1}{N}\sum_{n=1}^{N}\left(V_n(t) - \overline{V}_n(t)\right)^2} \tag{16}$$

GFP peak topomaps

Next, k-means clustering is performed on GFP Peaks maps. For resting state Microstates analysis, 4 distinct canonical Microstates are used (Khanna et al., 2015). For the mental arithmetic-based induced stress signals, data-driven Microstresses are based on the basis of subject-level and group-level clustering.

For the subject-level clustering, the topomaps from GFP peaks are extracted for each subject. These GFP tomomaps are then clustered for multiple K. The K-means clustering algorithm is applied multiple times (nRuns) with different initializations to mitigate the risk of convergence to local minima. To avoid the overlapping and keep the prominence of each map, a minimum distance of about 10 ms was kept between consecutive peaks. The percentile of the maximum threshold for selecting the highest peaks is set to be 80%.

Subject-level clustering

The centroids of each cluster are then selected for the group-level clustering. As a result of subject-level clustering, K×N maps were obtained, where N represents the number of subjects. To balance the contribution of each subject, all maps from K = 4 to K = 8 are pooled together to create a standard set of topomaps, which is then passed for group-level clustering (Fig. 7).

Now, for k = 8, correlation is computed to find the similarity between maps in which polarity is ignored using Eq. (19) (Fig. 8). In which way the maps with the high corr ($|r| > 0.9$, 90% similarity) are merged, which actually represents the same spatial configuration (Kleinert et al., 2024). Two pairs of group maps demonstrated strong correlations, specifically Map 1 and Map 2 (r = 0.911), as well as Map 4 and Map 5 (r = 0.917). These high correlation coefficients suggest a significant overlap in their spatial configurations.

Group-level clustering

After extracting the subject-level tentative Microstates (centroids), group-level clustering is applied to identify a data-driven set of representative Microstates. Now, the collected pool of all centroids [channels x (KxN)] from group-level clustering will be again clustered using K-means. The choice of K from K = 4 to 8 is consistent with prior literature (Tarailis et al., 2024). The range allows for capturing more robust Microstates without overfitting or underfitting.

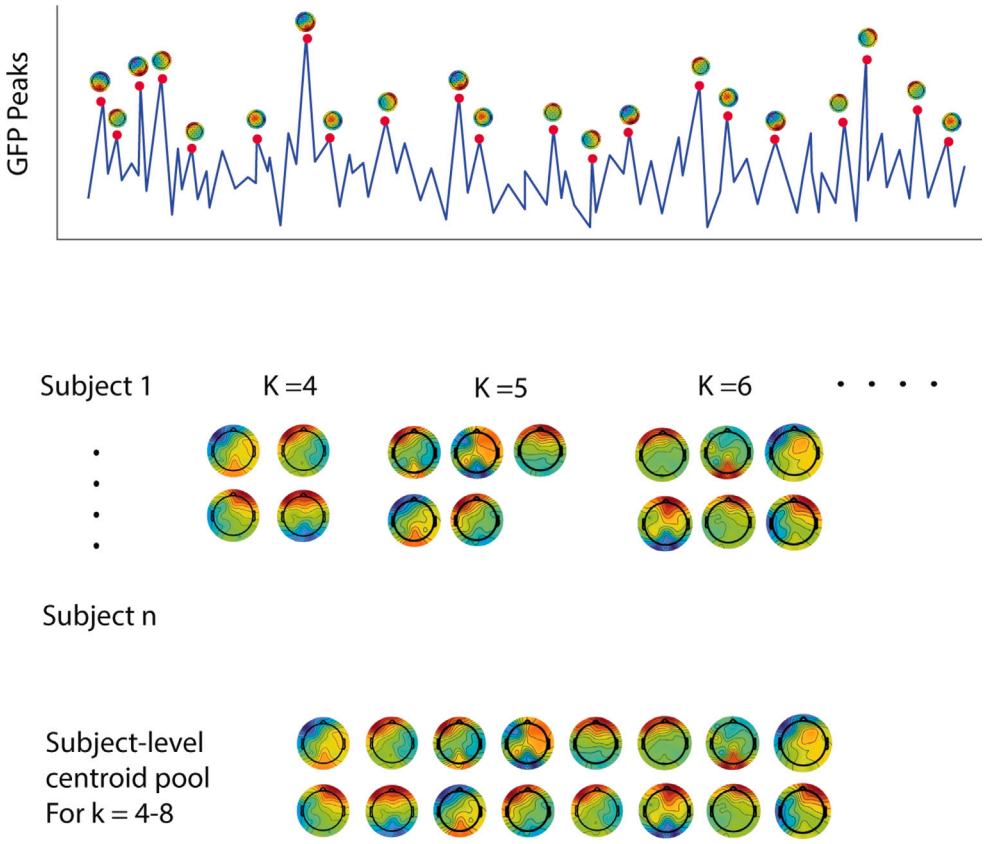

Fig. 7. (From top to bottom) The topomaps present at the GFP peaks are collected for all subjects n(80). For these, topomaps are clustered for K = 4 till K = 8 and the centroid of each clustering (K) is kept in a common, subject-level pool. Upon this final centroid pool, the group level clustering is applied.

Optimal K-clusters

For each K, the selection criteria for optimal k are computed using multiple ways. The cross-validation residual and global Explained Variance GEV (Michel & Koenig, 2018) are two of them. Global Explained Variance GEV value represents how closely a topomap at a particular time point best represents its assigned labels. The higher the GEV value, the better the maps are represented by the assigned labels.

$$\mathrm{GEV} = \frac{\sum_{t\in\mathcal{T}} \left[\mathrm{GFP}(t)\cdot r\left(V(t), M_{s(t)}\right)\right]^2}{\sum_{t\in\mathcal{T}} \mathrm{GFP}(t)^2} \tag{17}$$

where $V(t)$ denotes the scalp potential map at time t, $M_{s(t)}$ represents the centroid of the Microstate assigned to time t, and $r\left(V(t), M_{s(t)}\right)$ is the spatial correlation (often the absolute value is used during assignment).

The GFP weighting emphasizes time points with higher SNR, ensuring that high-variance moments contribute more to the explained variance. GEV tends to increase with increasing number of K as variance increases (Fig. 9) (Liu et al., 2024). However, increasing GEV tends to capture noise rather than useful information. To mitigate the limitations of GEV, a Cross-validation residual-like function is also used to find how well a model generalizes for those assigned labels. CV values minimizes the residual error for independent unseen subjects.

Let $\mathbf{X}_{n,i} \in \mathbb{R}^C$ denote the scalp topography (across C channels) at the ith GFP peak, and let $\hat{\mathbf{X}}_{n,i}$ be its reconstructed map, obtained by projecting $\mathbf{X}_{n,i}$ onto the corresponding Microstate centroid. The residual error between the original and reconstructed maps reflects the part of the signal that cannot be explained by the model. The cross-validation (CV) criterion is then defined as:

$$\mathrm{CV} = \frac{\sum_i \|\mathbf{X}_{n,i}\|^2}{\sum_i \|\mathbf{X}_{n,i} - \hat{\mathbf{X}}_{n,i}\|^2} \tag{18}$$

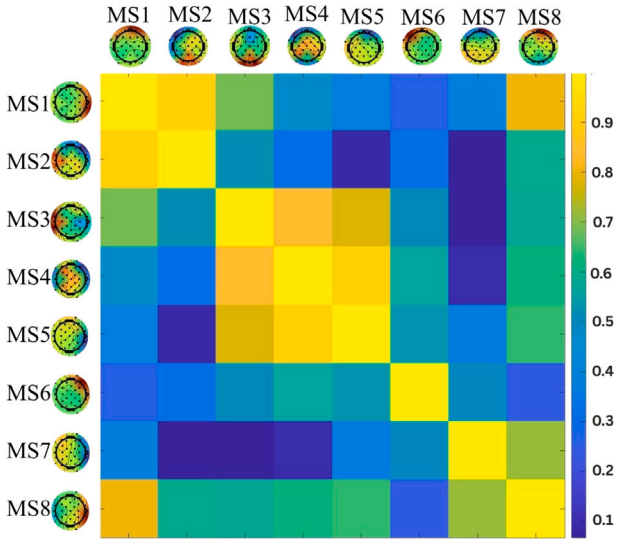

Fig. 8. The Pearson's correlation value between 8 topomaps presented in the form of an adjacency heat map. String correlation is observed between pairs of maps 1 and 2 and maps 4 and 5. The diagonal value gives 1, indicating the 100 correlation of a topomap with itself.

A lower CV value indicates a better reconstruction: The centroid can capture and reconstruct the underlying EEG signal. The lower value of CV means they are not overfit and generalizes well. In other words, GEV explains how closely a map is fitted by the label and CV residual value explains how well the assigned map generalizes across all subjects. This

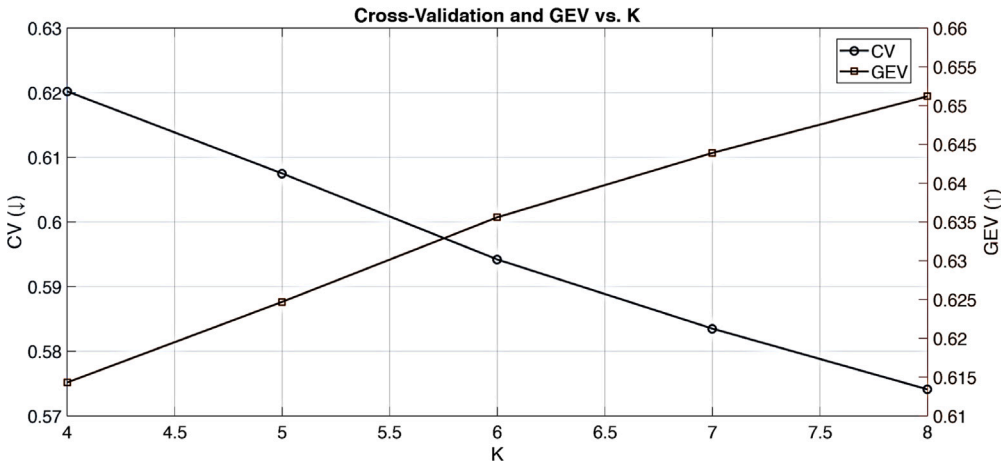

Fig. 9. GEV vs CV curve for each value of K from K = 4 to K =8. The minimum value of CV (0.614) and maximum value of GEV (0.652) is obtained for K = 8.

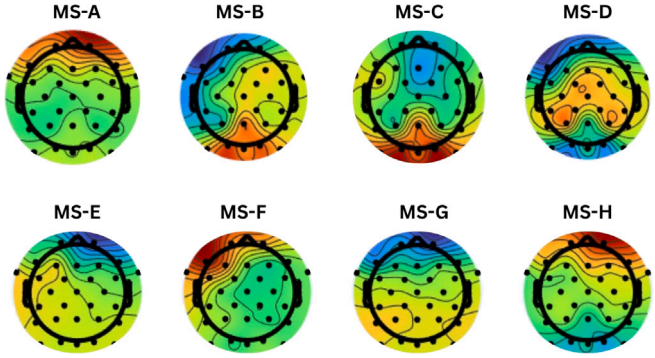

Fig. 10. 8 Topomaps centroids obtained after group-level clustering.

combination ensures that the Microstates are informative, stable and physiologically meaningful and robust.

Spatial merging of topographical maps

EEG brain maps acquired can be polarity invariant with each other, but their spatial pattern is the same (Pascual-Marqui et al., 1995). To mitigate the effect of correlated maps and resulting redundancy in cluster centroids, the maps with a correlation higher than a particular threshold are merged

$$\rho_{ij} = |r_{ij}| = \left| \frac{\sum_{k=1}^{N}(M_{k,i} - \bar{M}_i)(M_{k,j} - \bar{M}_j)}{\sqrt{\sum_{k=1}^{N}(M_{k,i} - \bar{M}_i)^2}\sqrt{\sum_{k=1}^{N}(M_{k,j} - \bar{M}_j)^2}} \right| \tag{19}$$

This data-driven approach helped extract a set of topomaps (Fig. 10) that carefully considers the underlying stressful brain dynamics. Now this final set of spatially distinct set of maps will be used to backfit into the GFP peaks of the individual subject.

Backfitting microstates

After obtaining the final set of Microstate templates, the backfitting is done to label each time point in the EEG with the best-matching template, enabling us to reconstruct the temporal sequence of Microstates across the recording (Fig. 11). To reduce spurious, short-lived fluctuations caused by noise or abrupt switching, temporal smoothing was applied to the sequence, enforcing a biologically plausible minimum duration for each Microstate. This combination of clustering, variance-based evaluation, and smoothing ensures that the identified Microstates are both statistically robust and neurophysiologically meaningful.

From the final Microstates, subject-wise temporal features are extracted as they provide how these transient patterns evolve. Temporal resolution of Microstates makes an ideal candidate to analyze fast changes in the brain. The key temporal parameters which are extracted for this research are (Tarailis et al., 2024): Mean duration, Occurrence Rate, Coverage and probability of transition from one state to another. Mean duration represents the average time a specific Microstate occurred. Occurrence rate records how frequently a specific Microstate appears per subject, per state. Coverage tells about how much of the total time is covered by each Microstate. Lastly, the transition probabilities describe how often a state switches between other states. All the temporal features collected for all signals are flattened into a vector and create a feature vector of an 80 × 54 matrix.

Multi-modal feature fusion using attention mechanism

Different modalities provide a unique representation of neural activity; however, their relative discriminative significance may vary across subjects or cognitive states. To effectively integrate these heterogeneous feature spaces, an attention-based fusion mechanism is employed.

Attention fusion (Fig. 12) is an effective way to fuse features which are derived from multiple modalities. Unlike traditional and simpler methods like averaging or concatenation, the attention mechanism carefully considers the modality-specific information, emphasizing only on more dominant patterns and suppressing the less important features.

Three distinct feature sets were fused using an attention mechanism. The Transfer Entropy feature is of dimensions W × 992, which represents the temporally derived statistical characteristics where W =1920 windows. For Microstates features the dimensions were N×54, where N = 80 signals. The Granger Causality is a set of N× i×j adjacency matrix where i and j are the number of channels. The given three feature sets have different dimensions, which makes them incompatible to feed into the latent space. To make distinct sets of modalities features consistent, the subject-level linear interpolation is done via Python's interp1D function for MS and GC features to meet the target dimensionality of Transfer Entropy. The interpolation function is defined as:

$$f_i(x) = y_i^{(\text{old})} + \frac{y_i^{(\text{new})} - y_i^{(\text{old})}}{x^{(\text{new})} - x^{(\text{old})}}(x - x^{(\text{old})}) \tag{20}$$

The obtained values were normalized to minimize the scaling discrepancies across all distinct feature sets.

To effectively integrate features from different neural modalities, a feature-level Attention-Based Fusion (ABF) model is used. This method provides an effective way to fuse heterogeneous feature sets from Granger Causality, Transfer Entropy and Temporal Microstate features. ABF performs feature-level fusion (Cai et al., 2020) using some learnable weights that dynamically modulate and select the most contributing features across all feature sets. First, the feature matrix MS, GC and TE are projected into a common latent space for modality-specific linear transformation to create embeddings for each feature set:

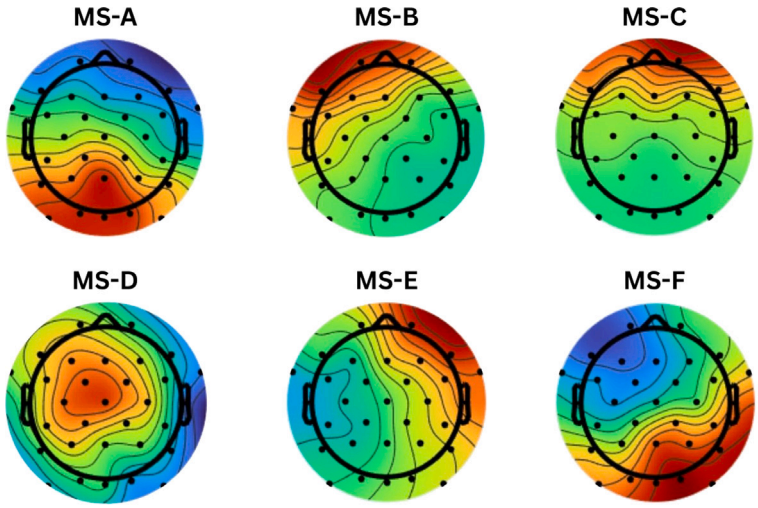

Fig. 11. 6 Final microstates obtained from 2 level clustering method for stress-based tasks.

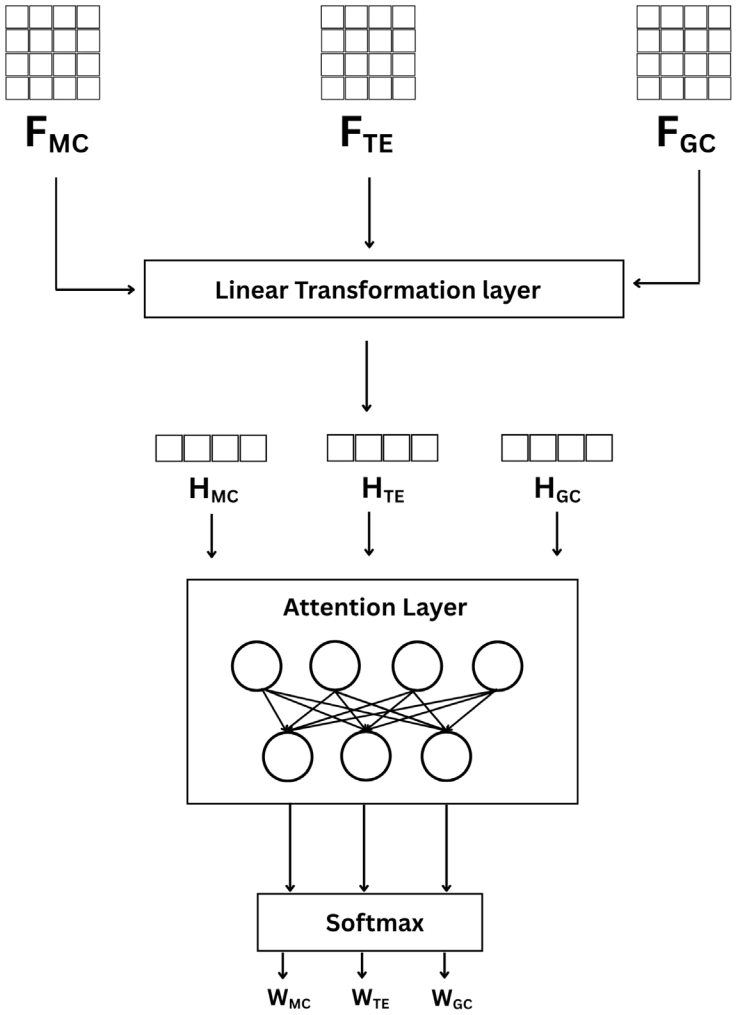

Fig. 12. Attention fusion model. F_{MC}, F_{TE} and F_{GC} are input feature sets. The linear transformation layer transforms the input into a linear embedding suitable for the attention layer. The attention layers compute and return the weight for each feature set, which are normalized using softmax.

Table 2
Key parameters and architectural details of SVM, LDA, and MLP classifiers.

SVM		LDA		MLP	
Parameter	Value	Parameter	Value	Parameter	Value
Kernel	Radial Basis Function (RBF)	Optimization	Solver	Hidden Layers	2
Regularization	$C = 1.0$	Regularization	Shrinkage	Hidden Units	(256, 128)
Kernel Width	Gamma (scale)	Search Method	Grid Search	Regularization	Dropout (0.4)
				Loss Function	Cross-Entropy

$$H_m = \tanh(W_m F_m + b_m), \quad \text{where } m \in \{\text{TE}, \text{MS}, \text{GC}\} \tag{21}$$

The transformed features H_m are fed into the self-attention layer, which computes the relevance score w_T for each type of feature. The softmax function normalizes the obtained score values, which represent the relative importance of each modality.

$$\alpha_m = \text{softmax}(w^\top H_m) \tag{22}$$

$$H_{\text{fused}} = \sum(\alpha_{\text{TE}} + \alpha_{\text{MS}} + \alpha_{\text{GC}}) \tag{23}$$

The attention layer helps learn the sample-weight dependent α_m. The final fused vector contains the discriminating features from all three modalities and is classified using LDA. Fig. 12 depicts the attention mechanism in detail. This fused feature set is then used to perform classification using Group 5-Fold classification with 32 subjects selected for training and 8 for testing. After creating the training and testing datasets, the attention fusion model is re-initialized to avoid information leakage. The reproducibility for same subject-specific folds is ensured across all experiments.

Classifiers

For the binary classification of signals into stress and relax states, three different classifiers are used to improve the reliability of the proposed methodology. The parametric and architectural details of classifiers is presented in Table no. 2. All three models are implemented using a Group 5-fold validation approach.

Support vector machine

Support Vector Machine (SVM) is a supervised Machine learning model that gives robust performance for classification and regression tasks. The core idea of SVM is to separate the given classes with the help of a hyperplane that maximizes the distance between datapoints from each class. In other words, the hyperplane that separates the given (two) classes is at the maximum distance from data points of each class. This helps in improving the generalization to unseen data. For the classification between stress and relax state using a fused feature set and considering the non-linearity of feature sets, a Radial Basis Function (RBF) kernel is used, which maps each dimension into an infinite feature space where linear separation is possible. The RBF kernel is given as:

$$K(x, y) = \exp\left(-\gamma \|x - y\|^2\right) \tag{24}$$

where, x and y are two feature points. the RBF is based on maximizing the distance between two feature points γ controls the rate at which the similarity between feature points decreases with the increasing distance.

Linear discriminant analysis

Linear Discriminant Analysis (LDA) is a supervised machine learning algorithm that is based on identifying a linear combination of features to separate classes. LDA is based on maximizing variance using class information. It works by projecting feature space onto a lower-dimensional subspace that maximizes the ratio of inter-class variance and intra-class variance. For an x feature vector with discriminant weights w, the linear combination of features is given by

$$y = \mathbf{w}^T \mathbf{x} + b \tag{25}$$

The optimal w is derived from the ratio of inter-class scatter matrix S_b and intra-class scatter matrix S_w.

$$\mathbf{w} = \arg\max_{\mathbf{w}} \frac{\mathbf{w}^T \mathbf{S}_b \mathbf{w}}{\mathbf{w}^T \mathbf{S}_w \mathbf{w}} \tag{26}$$

This criterion enhances the distinction between classes where features might be highly correlated and multidimensional. Before feeding into the classifier, the fused matrix is first imputed to handle missing values and normalize feature distribution.

Multi-layer perceptron

Multi-layer perception is a fully connected neural network that learns non-linear patterns from the given data by reducing the dimension progressively after each layer. Each layer is preceded by a ReLU activation function for preventing overfitting and add non-linearity. The hidden layers transform the feature set into lower dimensions based on the cross-entropy function. According to Eq. (27) at each level, where $\tilde{\mathbf{h}}_n$ is the features acquired from previous hidden layer and W is the weights.

$$\mathbf{h}_n = \sigma\left(\mathbf{W}_n \tilde{\mathbf{h}}_n + \mathbf{b}_n\right) \tag{27}$$

Performance evaluation

To evaluate the robustness of fused features, several standard classification matrices are used, including accuracy, precision, recall, F1 score, Area Under the Receiver Operating Characteristic Curve (AUC), and loss. Accuracy measures of correctness of classified labels. Precision is the proportion of correctly predicted positive samples among all samples which are predicted positive. Recall or sensitivity identify the actual possible cases. F1 score observes the balance between the prediction of each class label. AUC represents a threshold-independent measure of separability of classes (stress and relax).

$$\text{Accuracy} = \frac{TP + TN}{TP + TN + FP + FN} \tag{28}$$

where TP, TN, FP, and FN denote the number of true positives, true negatives, false positives, and false negatives, respectively.

$$\text{Precision} = \frac{TP}{TP + FP} \tag{29}$$

$$\text{Recall} = \frac{TP}{TP + FN} \tag{30}$$

$$F_1 = 2 \times \frac{\text{Precision} \times \text{Recall}}{\text{Precision} + \text{Recall}} \tag{31}$$

$$\text{AUC} = \int_0^1 TPR(FPR)\, d(FPR) \tag{32}$$

where TPR and FPR represent the True Positive Rate and False Positive Rate, respectively.

For binary classification, the binary cross-entropy loss is defined as:

$$\mathcal{L} = -\frac{1}{N} \sum_{i=1}^{N} \left[y_i \log(\hat{y}_i) + (1 - y_i) \log(1 - \hat{y}_i)\right] \tag{33}$$

where y_i denotes the true label, $\hat{y}_i$ is the predicted probability, and N is the total number of samples.

Table 3
Five-fold performance of the proposed attention-based fusion model for SVM.

Training						
Fold	Accuracy	Precision	Recall	F1-Score	AUC	Loss
1	0.9589	0.9619	0.9557	0.9588	0.9923	0.00521
2	0.9153	0.9381	0.8893	0.9131	0.9752	0.07031
3	0.9388	0.9365	0.9414	0.9389	0.9839	0.03646
4	0.9212	0.9284	0.9127	0.9205	0.9754	0.03646
5	0.9694	0.9724	0.9661	0.9693	0.9955	0.07552
Mean ± SD	**0.9407 ± 0.0028**	**0.9475 ± 0.0032**	**0.9330 ± 0.0040**	**0.9401 ± 0.0030**	**0.9845 ± 0.00001**	**0.0057 ± 0.0028**
Testing						
Fold	Accuracy	Precision	Recall	F1-Score	AUC	Loss
1	0.9948	0.9948	0.9948	0.9948	0.9996	0.0052
2	0.9297	0.8986	0.9688	0.9323	0.9843	0.0703
3	0.9635	0.9320	1.0000	0.9648	0.9985	0.0365
4	0.9609	0.9836	0.9375	0.9600	0.9961	0.0391
5	0.9245	0.9503	0.8958	0.9223	0.9812	0.0755
Mean ± SD	**0.9547 ± 0.0286**	**0.9519 ± 0.0390**	**0.9593 ± 0.0433**	**0.9548 ± 0.0287**	**0.9919 ± 0.0086**	**0.0453 ± 0.0286**

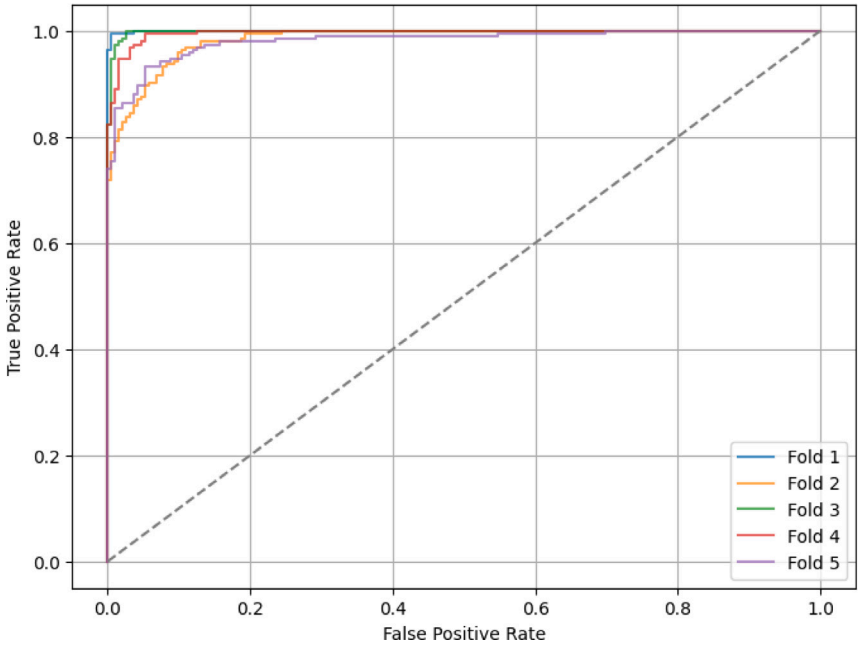

Fig. 13. Receiver operating characteristic curve for Group 5-Fold based classification using SVM.

Results and discussion

SVM classification results

The SVM classifier demonstrates high performance on both training and testing datasets (Table 3). The mean training accuracy is 0.9407 ± 0.0028, and the average testing accuracy is 0.9547 ± 0.0286, indicating strong generalization with minimal overfitting. Similarly, the AUC values are very high (0.9919 ± 0.0086 for testing), which reflects excellent class discrimination. The low loss values confirm stable convergence during training. Overall, the SVM with RBF kernel is highly effective for a fully fused feature dataset, due to its ability to handle non-linear separability in high-dimensional space.

Fig. 13 shows the ROC curves for all five cross-validation folds. These curves demonstrate consistent classification performance across all folds with slight variations. Each curve remains close to the top-left corner, which demonstrate the high true positive rates at very low false positive rates. In addition, minimal variations across folds indicate that the model has strong stability, robustness, and excellent generalization capability across different data splits. Similarly, confusion matrices across all folds are represented in Fig. 14.

LDA classification results

The testing accuracy reported by LDA is 0.9891 ± 0.0137, as presented in Table 4. This indicates that LDA gives robust generalization with very low variance. LDA also shows high precision and recall, suggesting it is effective in identifying both classes correctly. However, LDA is inherently a linear classifier, and while the current dataset appears to be linearly separable to a large extent, it may not capture complex nonlinear relationships. To further confirm the robustness of the fused feature set, the classification is performed using MLP.

To further validate the discriminative capability of the fusion model, AUC–ROC curves were plotted for each test fold, as shown in Fig. 15. The ROC curves illustrate the relationship between the True Positive Rate (TPR) and the False Positive Rate (FPR) under varying decision thresholds. Across all folds, the model consistently achieved high AUC values, indicating high class separability. Fig. 16 showing the confusion

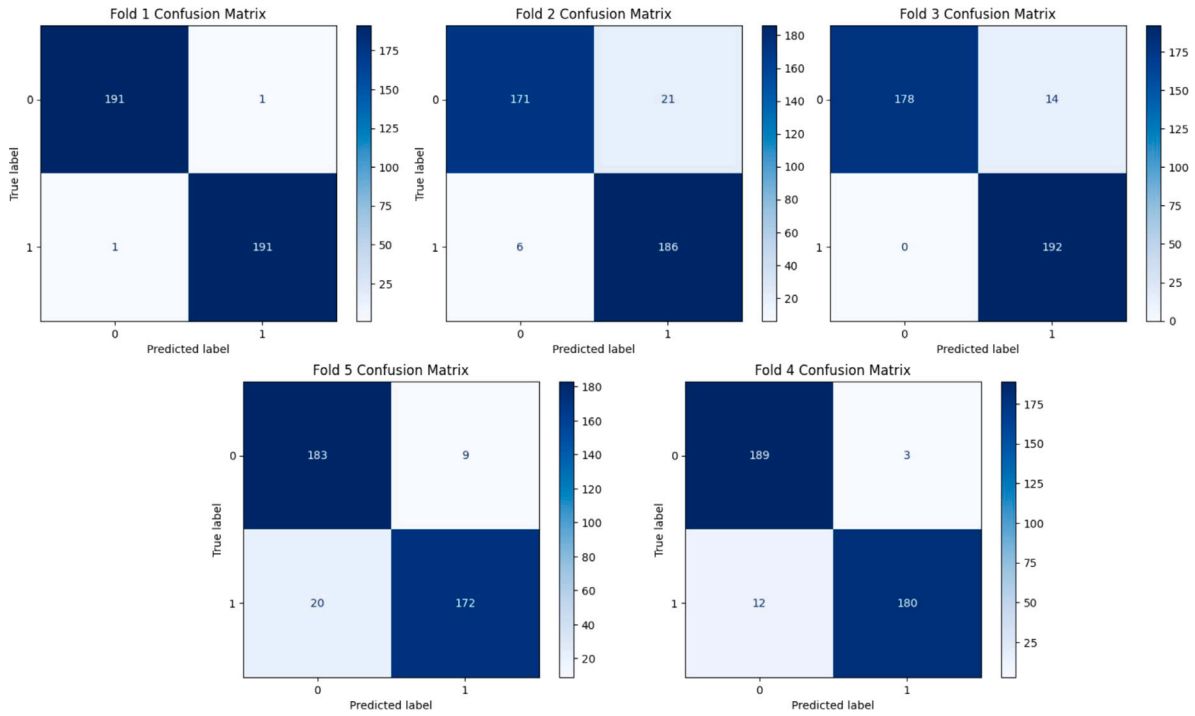

Fig. 14. Confusion matrix for Group 5-Fold based classification using SVM.

Table 4
Five-fold performance of the proposed attention-based fusion model for LDA.

Training						
Fold	Accuracy	Precision	Recall	F1-Score	AUC	Loss
1	0.9967	0.9974	0.9961	0.9967	0.9999	0.0033
2	0.9935	0.9948	0.9922	0.9935	0.9996	0.0065
3	0.9954	0.9948	0.9961	0.9954	0.9999	0.0046
4	0.9909	0.9948	0.9870	0.9909	0.9994	0.0091
5	0.9928	0.9974	0.9883	0.9928	0.9996	0.0072
Mean ± SD	**0.9939 ± 0.0023**	**0.9958 ± 0.0014**	**0.9919 ± 0.0043**	**0.9939 ± 0.0023**	**0.9997 ± 0.0002**	**0.0061 ± 0.0023**
Testing						
Fold	Accuracy	Precision	Recall	F1-Score	AUC	Loss
1	0.9688	0.9545	0.9844	0.9692	0.9970	0.0313
2	0.9974	0.9948	1.0000	0.9974	1.0000	0.0026
3	0.9818	0.9894	0.9740	0.9816	0.9967	0.0182
4	1.0000	1.0000	1.0000	1.0000	1.0000	0.0000
5	0.9974	0.9948	1.0000	0.9974	1.0000	0.0026
Mean ± SD	**0.9891 ± 0.0137**	**0.9867 ± 0.0186**	**0.9917 ± 0.0126**	**0.9891 ± 0.0137**	**0.9987 ± 0.0016**	**0.0109 ± 0.0137**

matrices for different folds, also indicate good performance with very few false positives and false negatives.

MLP classification results

The training accuracy reported by MLP is 0.9074 ± 0.0235, and testing accuracy is 0.8349 ± 0.0636 in Table 5, which is slightly lower than both SVM and LDA. The higher standard deviation in testing metrics suggests that the MLP model exhibits greater sensitivity to data splits, due to its higher learnability and the risk of overfitting in relatively small datasets. Nevertheless, the MLP achieves competitive F1 scores and AUC values, indicating that it still captures meaningful non-linear patterns in the data.

The ROC curves across the five folds, in Fig. 17, indicate good overall classification performance, though with greater variability compared to the previous figure. While most folds achieve high true positive rates at relatively low false positive rates, some curves rise more gradually, suggesting moderate differences in discriminative capability and slightly reduced stability across data splits. Performance of MLP is poor than SVM and LDA, as indicated by the number of wrong predictions in Fig. 18.

Tables 3, 4, and 5 present the classification performances (Training) across all five folds for SVM, MLP and LDA, respectively. The results confirm that the proposed fusion approach effectively mitigates overfitting and preserves the discriminative power across subjects.

Ablation study

To compare the effectiveness of fused features, the classification results of the fused feature set are compared with the individual feature set. The classification results obtained from individual features from Transfer Entropy TE, Microstates MS, and Granger Causality GC showed overall moderate performances in Tables 6, 7 and 8 for SVM, LDA and MLP respectively. Each set of feature modalities captures a distinct brain functional state.

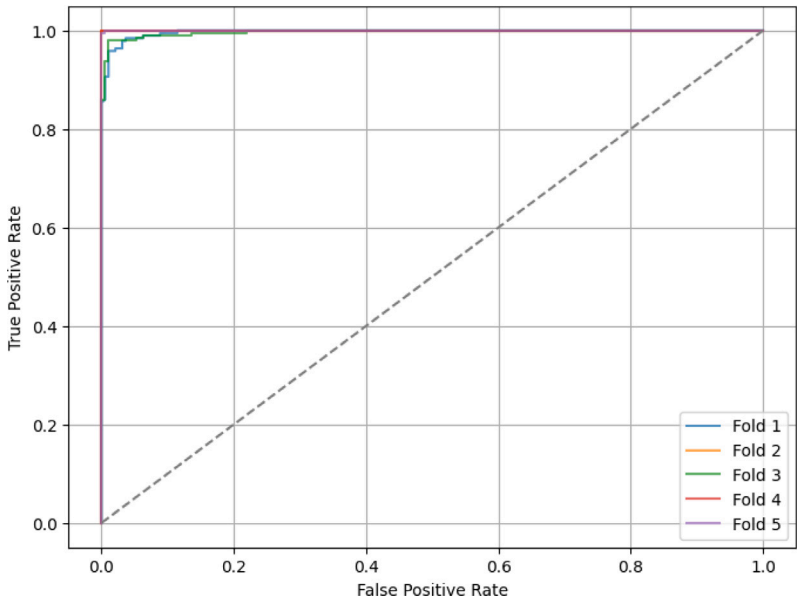

Fig. 15. Receiver operating characteristic curve for Group 5-Fold based classification using LDA.

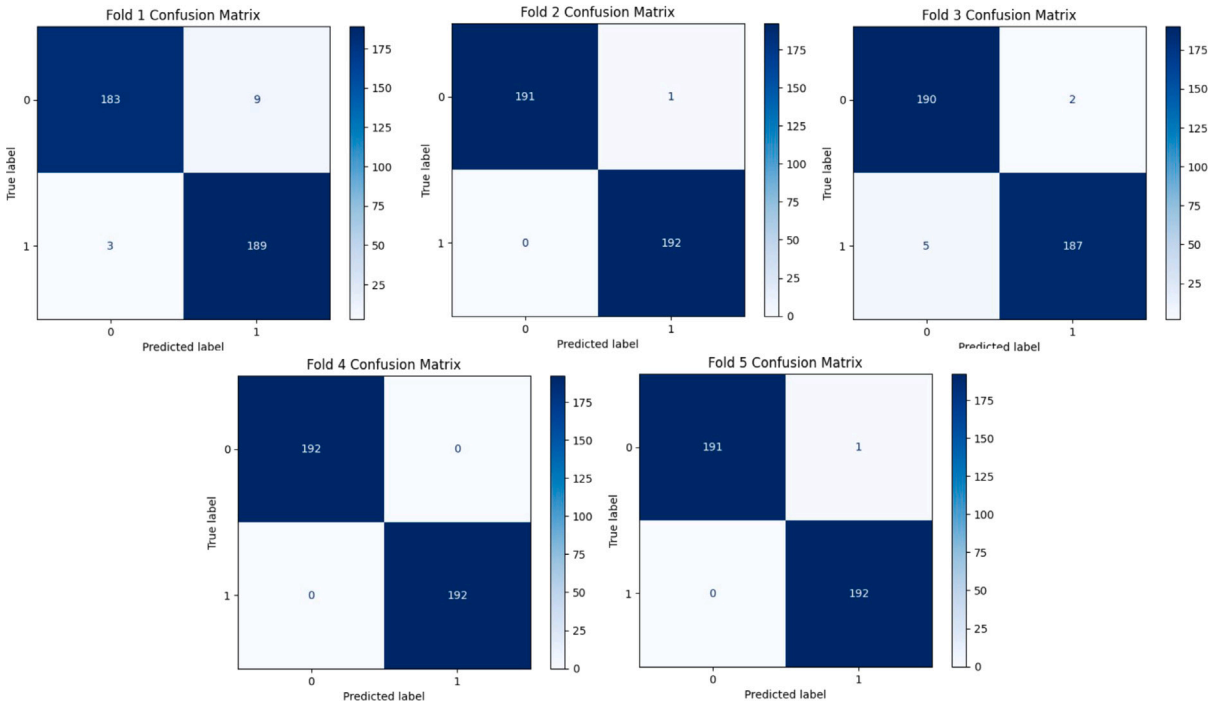

Fig. 16. Confusion matrix for Group 5-Fold based classification using LDA.

Among all three classifiers, the Microstate features gave the highest classification performance with SVM, with a mean accuracy of 0.6125 ± 0.0745. Despite capturing the transient topographical configurations of brain activity, the results indicate inconsistent generalization, suggesting that Microstate dynamics alone may not sufficiently represent the discriminative temporal dependencies required for robust stress-relax separation.

The Granger Causality features achieved highest accuracy of 0.8695 ± 0.0723 and an AUC of 0.9339 ± 0.0406 for MLP. While GC captures linear causal relationships among EEG channels, its performance remained below that of TE, reflecting its limitation in modeling nonlinear information transfer.

TE features emerge as the most powerful and reliable descriptors for this classification task. Supporting their integration into multimodal fusion frameworks for enhanced EEG-based discrimination. For all three classifiers and for all three feature sets obtained from different modalities, a similar behavior was observed, depicted by each feature set. However, combining these features using an attention mechanism

Table 5
Group 5-Fold based performance of the proposed attention-based fusion model for MLP.

Training						
Fold	Accuracy	Precision	Recall	F1-Score	AUC	Loss
1	0.9287	0.9067	0.9689	0.8973	0.9379	0.0713
2	0.9349	0.9987	0.9389	0.9087	0.9281	0.0651
3	0.8934	0.9671	0.8678	0.8209	0.9190	0.1066
4	0.8799	0.8978	0.8456	0.8480	0.9876	0.1201
5	0.9001	0.8587	0.9467	0.8097	0.9182	0.0999
Mean ± SD	**0.9074 ± 0.0235**	**0.9258 ± 0.0556**	**0.9136 ± 0.0498**	**0.8569 ± 0.0410**	**0.9382 ± 0.0281**	**0.0926 ± 0.0235**
Testing						
Fold	Accuracy	Precision	Recall	F1-Score	AUC	Loss
1	0.8802	0.8174	0.9792	0.8910	0.9723	0.1198
2	0.7396	0.6949	0.8542	0.7664	0.9021	0.2604
3	0.8776	0.8680	0.8906	0.8792	0.9520	0.1224
4	0.7969	0.7767	0.8333	0.8040	0.9071	0.2031
5	0.8802	0.9506	0.8021	0.8701	0.9607	0.1198
Mean ± SD	**0.8349 ± 0.0636**	**0.8215 ± 0.0950**	**0.8719 ± 0.0691**	**0.8423 ± 0.0566**	**0.9388 ± 0.0307**	**0.1651 ± 0.0636**

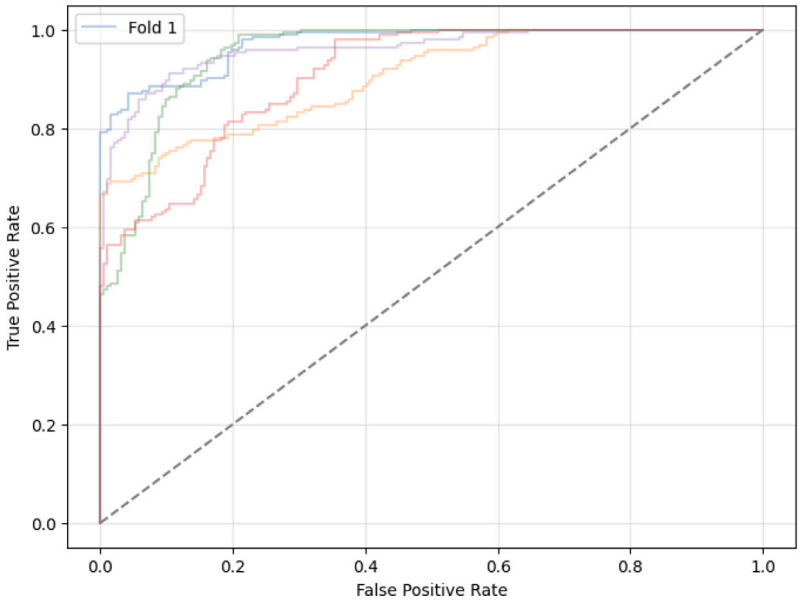

Fig. 17. Receiver operating characteristic curve for Group 5-Fold based classification using MLP.

carefully extracts the most effective features from all three modalities to provide more powerful and robust classification, as explained in earlier sections.

Granger causality and transfer entropy fusion

The fusion of Transfer Entropy and Granger Causality features yielded a significant performance in classification performance compared to the individual modalities. As shown in Tables 9–11 the combined TE+GC model achieved a mean testing accuracy of 0.9526 ± 0.0453, F1-score of 0.9497 ± 0.0416, and an exceptionally high AUC of 0.9803 ± 0.0245 using SVM Model, demonstrating strong generalization and discriminative capability across folds. This improvement suggests that fusing nonlinear (Transfer Entropy) and linear (Granger Causality) causal dynamics provides a more comprehensive characterization of effective brain connectivity, capturing both complex directional information flow and stable causal dependencies.

The three ROC plots, in Fig. 19, illustrate varying levels of classification performance across the five folds. The best performance is illustrated in middle plot which is for SVM model. It demonstrates excellent and highly consistent performance, with curves closely approaching the top-left corner. These curves indicate high true positive rates at very low false positive rates. In contrast, the left plot shows moderate performance with noticeable variability among folds, suggesting less stable generalization. The right plot reflects good overall discrimination, though some folds rise more gradually, indicating moderate differences in sensitivity across data splits.

Granger causality and microstates fusion

The performance results of the Microstates Features, and Granger Causality features indicate moderate discriminative capability during training and limited generalization on the test data, as shown in Tables 12–14. During training, the model achieved an average accuracy of 0.7891 ± 0.0614, precision of 0.7874 ± 0.0545, recall of 0.7958 ± 0.0849, and an F1 score of 0.7899 ± 0.067, with a mean AUC of 0.8419 for MLP. For SVM, an average accuracy was obtained to be 70.00%.

These values suggest that the extracted features were able to capture meaningful class-specific patterns to some extent. However, the testing phase shows a considerable performance drop. Table 14 shows a similar behavior by SVM, which depicts that MS and GC are not complementary when fused. This discrepancy between training and testing results may indicate potential overfitting or that the MS and GC features alone are not sufficiently robust for distinguishing between the two classes.

The comparative ROC analysis across three models in Fig. 20, reveals distinct performance patterns. The first model exhibits moderate

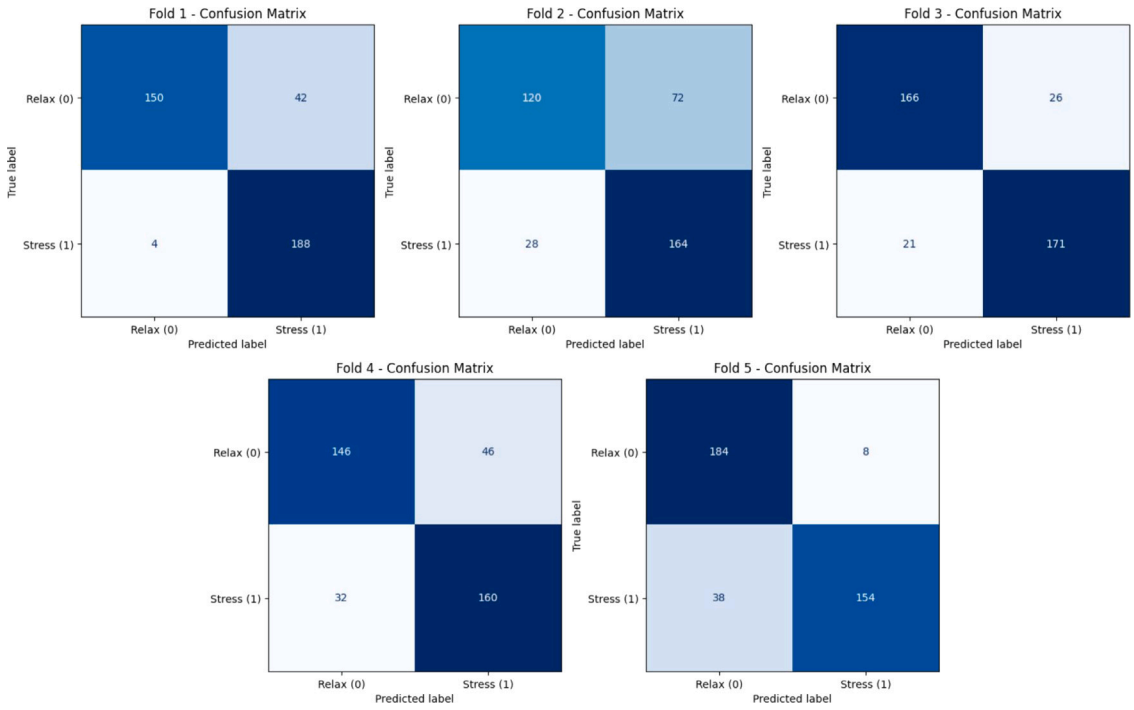

Fig. 18. Confusion matrix for 5-fold cross-validation-based classification using MLP.

Table 6
Group 5-Fold based performance of individual feature modalities using SVM.

Granger Causality Features						
Fold	Accuracy	Precision	Recall	F1-Score	AUC	Loss
1	0.6250	0.6000	0.7500	0.6667	0.3281	0.3750
2	0.6875	0.7143	0.6250	0.6667	0.4062	0.3125
3	0.5000	0.5000	0.5000	0.5000	0.4844	0.5000
4	0.7500	0.7500	0.7500	0.7500	0.2812	0.2500
5	0.6250	0.6000	0.7500	0.6667	0.2969	0.3750
Mean ± SD	**0.6375 ± 0.0919**	**0.6329 ± 0.1003**	**0.6750 ± 0.1118**	**0.6500 ± 0.0913**	**0.3594 ± 0.0855**	**0.3625 ± 0.0919**
Transfer Entropy Features						
Fold	Accuracy	Precision	Recall	F1-Score	AUC	Loss
1	0.5339	0.5528	0.3542	0.4317	0.5660	0.4661
2	0.5573	0.5705	0.4635	0.5115	0.5889	0.4427
3	0.5000	0.5000	0.5417	0.5200	0.4768	0.5000
4	0.4740	0.4597	0.2969	0.3608	0.4562	0.5260
5	0.4974	0.4969	0.4167	0.4533	0.5045	0.5026
Mean ± SD	**0.5125 ± 0.0344**	**0.5160 ± 0.0446**	**0.4146 ± 0.0961**	**0.4555 ± 0.0635**	**0.5185 ± 0.0581**	**0.4875 ± 0.0344**
Microstates Features						
Fold	Accuracy	Precision	Recall	F1-Score	AUC	Loss
1	0.6250	0.6000	0.7500	0.6667	0.2344	0.3750
2	0.5625	0.5556	0.6250	0.5882	0.5000	0.4375
3	0.6875	0.6667	0.7500	0.7059	0.2188	0.3125
4	0.6875	0.6667	0.7500	0.7059	0.3281	0.3125
5	0.5000	0.5000	0.3750	0.4286	0.4688	0.5000
Mean ± SD	**0.6125 ± 0.0745**	**0.5978 ± 0.0709**	**0.6500 ± 0.1500**	**0.6191 ± 0.1104**	**0.3509 ± 0.1113**	**0.3875 ± 0.0745**

discrimination with noticeable inter-fold variability. The second model demonstrates unstable and inconsistent behavior, with some folds approaching random classification. In contrast, the third model achieves superior and consistent performance, with curves concentrated near the top-left corner, indicating robust generalization and higher predictive reliability.

Transfer entropy and microstates fusion

The fusion of Microstate and Transfer Entropy features demonstrates a highly effective representation of EEG dynamics, resulting in strong discriminative performance for LDA, MLP and SVM as presented in Tables 15–17. The average training accuracy of 0.8008 ± 0.0345 with an AUC of 0.8642 ± 0.0324 indicates that the model effectively learned class-specific temporal and spatial patterns from the fused features when classified using LDA. The mean testing accuracy of 0.6266 ± 0.1360 and F1 score of 0.6419 ± 0.1182 confirm the robustness and generalization capability of the fusion approach. Upon evaluation of other related parameters, it is observed that Transfer Entropy outperformed the binary as well as full-fusion of features for MLP.

The superior performance of fusion, compared to the individual modalities (Microstates or, Transfer Entropy alone) demonstrates that

Table 7
Group 5-fold based performance of Individual feature modalities LDA.

Granger Causality Features						
Fold	Accuracy	Precision	Recall	F1-Score	AUC	Loss
1	0.6667	0.6798	0.6302	0.6541	0.7595	0.3333
2	0.5365	0.5729	0.2865	0.3819	0.5735	0.4635
3	0.6901	0.6973	0.6719	0.6844	0.7689	0.3099
4	0.8073	0.7783	0.8594	0.8168	0.7718	0.1927
5	0.6771	0.6382	0.8177	0.7169	0.7402	0.3229
Mean ± SD	**0.6753 ± 0.0934**	**0.6733 ± 0.0693**	**0.6335 ± 0.2010**	**0.6500 ± 0.1574**	**0.7228 ± 0.0884**	**0.3245 v 0.0972**
Microstates Features						
Fold	Accuracy	Precision	Recall	F1-Score	AUC	Loss
1	0.5651	0.5796	0.4740	0.5215	0.5951	0.4349
2	0.4740	0.4777	0.5573	0.5144	0.4740	0.5260
3	0.5625	0.5432	0.7865	0.6426	0.5382	0.4375
4	0.5365	0.5350	0.5573	0.5459	0.5338	0.4635
5	0.5339	0.5596	0.3177	0.4053	0.5666	0.4661
Mean ± SD	**0.5420 ± 0.0373**	**0.5392 ± 0.0367**	**0.5387 ± 0.1579**	**0.5259 ± 0.0920**	**0.5412 ± 0.0440**	**0.4578 ± 0.0353**
Transfer Entropy Features						
Fold	Accuracy	Precision	Recall	F1-Score	AUC	Loss
1	0.8281	0.8938	0.7448	0.8125	0.8685	0.1719
2	0.6536	0.6725	0.5990	0.6336	0.6697	0.3464
3	0.6250	0.6200	0.6458	0.6327	0.6397	0.3750
4	0.7344	0.7778	0.6563	0.7119	0.7807	0.2656
5	0.6615	0.6582	0.6719	0.6649	0.6113	0.3385
Mean ± SD	**0.7005 ± 0.0885**	**0.7249 ± 0.1154**	**0.6636 ± 0.0535**	**0.6717 ± 0.0751**	**0.6941 ± 0.1042**	**0.2995 ± 0.0613**

Table 8
Group 5-fold based performance of individual feature modalities using MLP.

Granger Causality Features						
Fold	Accuracy	Precision	Recall	F1-Score	AUC	Loss
1	0.8490	0.8988	0.7865	0.8389	0.9034	0.1520
2	0.7630	0.7919	0.7135	0.7507	0.8534	0.2370
3	0.9505	1.0000	0.9010	0.9479	0.9459	0.0495
4	0.9010	0.8738	0.9375	0.9045	0.9523	0.0990
5	0.8828	0.8210	0.9792	0.8931	0.9790	0.1172
Mean ± SD	**0.8695 ± 0.0723**	**0.8771 ± 0.0800**	**0.8635 ± 0.0866**	**0.8670 ± 0.0767**	**0.9260 ± 0.0480**	**0.1329 ± 0.0676**
Transfer Entropy Features						
Fold	Accuracy	Precision	Recall	F1-Score	AUC	Loss
1	0.9427	0.9885	0.8958	0.9399	0.9559	0.0573
2	0.8958	0.9000	0.8906	0.8953	0.9730	0.1042
3	0.8359	0.8525	0.8125	0.8320	0.8839	0.1641
4	0.8464	0.8446	0.8490	0.8468	0.9469	0.1536
5	0.8307	0.8009	0.8802	0.8387	0.9100	0.1693
Mean ± SD	**0.8703 ± 0.0549**	**0.8773 ± 0.0736**	**0.8656 ± 0.0319**	**0.8705 ± 0.0418**	**0.9339 ± 0.0406**	**0.1297 ± 0.0455**
Microstates Features						
Fold	Accuracy	Precision	Recall	F1-Score	AUC	Loss
1	0.4896	0.4895	0.4844	0.4869	0.4680	0.5104
2	0.4844	0.4831	0.4479	0.4649	0.4465	0.5156
3	0.4948	0.4958	0.6094	0.5467	0.4918	0.5052
4	0.5599	0.5673	0.5052	0.5344	0.5663	0.4401
5	0.5651	0.5839	0.4531	0.5103	0.5606	0.4349
Mean ± SD	**0.5186 ± 0.0367**	**0.5239 ± 0.0411**	**0.5003 ± 0.0681**	**0.5086 ± 0.0315**	**0.5066 ± 0.0485**	**0.4712 ± 0.0367**

combining microstate-based temporal. Stability with the directional information flow captured by transfer entropy provides a more comprehensive feature space, leading to enhanced classification performance.

The ROC curves across the three models, in Fig. 21, indicate moderate and variable classification performance. In the first plot, several folds remain close to the diagonal, suggesting limited discriminative ability, while one fold performs comparatively better. The second plot shows improved but inconsistent performance across folds. The third plot demonstrates relatively stronger and more stable discrimination, with most folds achieving higher true positive rates at lower false positive rates, indicating comparatively better generalization.

Results analysis

Among the three different feature sets, Transfer Entropy achieved the highest discriminating results with the accuracy of 87% as compared to the other two feature sets, Granger Causality (86%) and Microstates features (54%) for MLP. This tells us that TE is efficient in capturing the non-linearity between different neuronal regions while the brain is undergoing strong mental activity, which increases the stress level. GC, however, tried to build the linear causal link between brain regions. In contrast to this, microstates showed lower accuracies of 51%, which indicate limited performance. These results indicate

Table 9
Group 5-Fold based training and testing performance of the proposed SVM classifier using combined Transfer Entropy (TE) and Granger Causality (GC) features.

Training Performance						
Fold	Accuracy	Precision	Recall	F1-Score	AUC	Loss
1	0.8743	0.8890	0.8555	0.8719	0.9467	0.1257
2	0.9479	0.9574	0.9375	0.9474	0.9887	0.0521
3	0.9661	0.9735	0.9583	0.9659	0.9929	0.0339
4	0.9616	0.9683	0.9544	0.9613	0.9944	0.0384
5	0.9297	0.9447	0.9128	0.9285	0.9825	0.0703
Mean ± SD	**0.9351 ± 0.0358**	**0.9460 ± 0.0354**	**0.9235 ± 0.0370**	**0.9354 ± 0.0344**	**0.9813 ± 0.0192**	**0.0641 ± 0.0330**
Testing Performance						
Fold	Accuracy	Precision	Recall	F1-Score	AUC	Loss
1	1.0000	1.0000	1.0000	1.0000	1.0000	0.0000
2	0.9688	0.9787	0.9583	0.9684	0.9945	0.0312
3	0.8854	0.9744	0.7917	0.8736	0.9331	0.1146
4	0.9375	0.9667	0.9063	0.9355	0.9779	0.0625
5	0.9714	0.9840	0.9583	0.9710	0.9958	0.0286
Mean ± SD	**0.9526 ± 0.0453**	**0.9807 ± 0.0103**	**0.9229 ± 0.0840**	**0.9497 ± 0.0416**	**0.9803 ± 0.0245**	**0.0474 ± 0.0386**

Table 10
Group 5-Fold based training and testing performance of the proposed LDA classifier using combined Transfer Entropy (TE) and Granger Causality (GC) features.

Training Performance						
Fold	Accuracy	Precision	Recall	F1-Score	AUC	Loss
1	0.8874	0.8940	0.8789	0.8864	0.9594	0.1126
2	0.8333	0.8055	0.8789	0.8406	0.9257	0.1667
3	0.7500	0.7270	0.8008	0.7621	0.8356	0.2500
4	0.8568	0.8495	0.8672	0.8582	0.9201	0.1432
5	0.8346	0.8002	0.8919	0.8436	0.9152	0.1654
Mean ± SD	**0.8324 ± 0.0504**	**0.8152 ± 0.0644**	**0.8637 ± 0.0379**	**0.8182 ± 0.0465**	**0.9116 ± 0.0448**	**0.1676 ± 0.0481**
Testing Performance						
Fold	Accuracy	Precision	Recall	F1-Score	AUC	Loss
1	0.6068	0.5735	0.8333	0.6794	0.7740	0.3932
2	0.6484	0.6278	0.7292	0.6747	0.7465	0.3516
3	0.5885	0.5733	0.6927	0.6274	0.5946	0.4115
4	0.6823	0.8070	0.4792	0.6013	0.6604	0.3177
5	0.6667	0.6739	0.6458	0.6596	0.7225	0.3333
Mean ± SD	**0.6385 ± 0.0349**	**0.6519 ± 0.1007**	**0.6560 ± 0.1405**	**0.6487 ± 0.0310**	**0.6997 ± 0.0727**	**0.3615 ± 0.0381**

Table 11
Group 5-Fold based training and testing performance of the proposed MLP classifier using combined Transfer Entropy (TE) and Granger Causality (GC) features.

Training Performance						
Fold	Accuracy	Precision	Recall	F1-Score	AUC	Loss
1	0.9590	0.9608	0.9570	0.9589	0.9894	0.0410
2	0.9661	0.9520	0.9818	0.9667	0.9965	0.0339
3	0.9753	0.9854	0.9648	0.9750	0.9964	0.0247
4	0.9583	0.9757	0.9401	0.9576	0.9934	0.0417
5	0.9186	0.8935	0.9505	0.9211	0.9780	0.0814
Mean ± SD	**0.9551 ± 0.0204**	**0.9535 ± 0.0361**	**0.9585 ± 0.0165**	**0.9551 ± 0.0195**	**0.9902 ± 0.0079**	**0.0445 ± 0.0204**
Testing Performance						
Fold	Accuracy	Precision	Recall	F1-Score	AUC	Loss
1	0.6901	0.6398	0.8698	0.7373	0.7551	0.3099
2	0.7318	0.7032	0.8021	0.7494	0.8372	0.2682
3	0.6901	0.7325	0.5990	0.6590	0.7416	0.3099
4	0.7031	0.7321	0.6406	0.6833	0.8225	0.2969
5	0.7031	0.7532	0.6042	0.6705	0.7994	0.2969
Mean ± SD	**0.7036 v 0.0166**	**0.7122 ± 0.0451**	**0.7033 ± 0.1015**	**0.6999 ± 0.0414**	**0.7913 v 0.0343**	**0.2956 ± 0.0172**

that individual features are not sufficient to capture underlying neural dynamics when classified using MLP.

This may be because the cortical region is under highly non-linear intrinsic interactions, which result in diminishing its linear properties. The microstate captured in stressful conditions is a relatively newer direction. We obtained new sets of topographical maps with a defined methodology that carefully represents the brain images in stressful states. The discriminating power of microstates indicates that the obtained quasi-stable brain configurations may lack the fine-grained temporal dependencies for discrimination when in isolation.

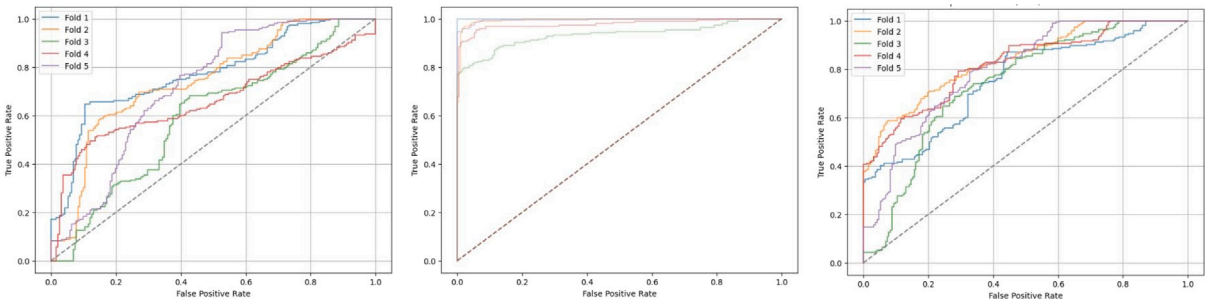

Fig. 19. ROC curves for group 5-fold based validation for TE and GC fusion. LDA (left), SVM (center), MLP (right).

Table 12
Group 5-Fold based training and testing performance of the proposed SVM classifier using combined Microstates (MS) and Granger Causality (GC) features.

Training Performance						
Fold	Accuracy	Precision	Recall	F1-Score	AUC	Loss
1	0.8438	0.8235	0.8750	0.8485	0.0713	0.1562
2	0.9375	0.9375	0.9375	0.9375	0.9922	0.0625
3	0.9688	1.0000	0.9375	0.9677	0.0000	0.0312
4	0.8750	0.8750	0.8750	0.8750	0.0723	0.1250
5	0.8125	0.8571	0.7500	0.8000	0.1328	0.1875
Mean ± SD	**0.8879 ± 0.0613**	**0.8780 ± 0.0681**	**0.8750 ± 0.0670**	**0.8657 ± 0.0625**	**0.2531 ± 0.4127**	**0.1321 ± 0.0569**
Testing Performance						
Fold	Accuracy	Precision	Recall	F1-Score	AUC	Loss
1	0.7500	0.7000	0.8750	0.7778	0.1250	0.2500
2	0.6250	0.5714	1.0000	0.7273	0.8281	0.3750
3	0.7500	0.8333	0.6250	0.7143	0.1406	0.2500
4	0.8125	0.8571	0.7500	0.8000	0.1094	0.1875
5	0.5625	0.6667	0.2500	0.3636	0.3281	0.4375
Mean ± SD	**0.7000 ± 0.0870**	**0.7257 ± 0.1047**	**0.7000 ± 0.2735**	**0.6766 ± 0.1726**	**0.3063 ± 0.2954**	**0.3000 ± 0.0870**

Table 13
Group 5-Fold based training and testing performance of the proposed LDA classifier using combined Microstates (MS) and Granger Causality (GC) features.

Training						
Fold	Accuracy	Precision	Recall	F1-Score	AUC	Loss
1	0.9206	0.9228	0.9180	0.9204	0.9641	0.0794
2	0.8613	0.8413	0.8906	0.8653	0.9429	0.1387
3	0.8542	0.8358	0.8815	0.8580	0.9331	0.1458
4	0.8757	0.8611	0.8958	0.8781	0.9367	0.1243
5	0.8945	0.8976	0.8906	0.8941	0.9479	0.1055
Mean ± SD	**0.8819 ± 0.0285**	**0.8713 ± 0.0382**	**0.8951 ± 0.0282**	**0.8832 ± 0.0265**	**0.9445 ± 0.0119**	**0.1187 ± 0.0253**
Testing Performance						
Fold	Accuracy	Precision	Recall	F1-Score	AUC	Loss
1	0.6823	0.6434	0.8177	0.7202	0.7190	0.3177
2	0.6901	0.6798	0.7188	0.6987	0.8048	0.3099
3	0.5000	0.5000	0.4896	0.4947	0.4796	0.5000
4	0.6224	0.6667	0.4896	0.5646	0.6088	0.3776
5	0.7188	0.7561	0.6458	0.6966	0.7457	0.2812
Mean ± SD	**0.6427 ± 0.0820**	**0.6492 ± 0.0949**	**0.6323 ± 0.1375**	**0.6350 ± 0.0860**	**0.6710 ± 0.1237**	**0.3573 ± 0.0856**

The fusion of GC and TE using an attention mechanism outperformed the individual discriminating power of both feature sets only for the SVM model. For the remaining Models, MLP and LDA, the binary fusion performs worse than these individual features. This indicates that GC's linear and TE's non-linear capabilities degrade the overall holistic effective connectivity. The fusion of GC and MS degraded the performance as compared to their individual feature sets. It reflects the temporal-resolution disparity between GC and MS. GC, which is based on time-series causality and Microstates, based on spatial–temporal clustering, introduce extract noise during fusion. Moreover, a significant degradation in performance can be seen for various other binary pairs. For example, MS + TE showed the accuracy of 62.66%, which is worse to a significant extent when compared with their individual counterparts. A similar pattern can be observed with MS + GC, which fails to improve and suggests a weak synergy between the two features.

The ablation study and classification results presented by fusing all features suggest that the fully fused features give improved classification results when classified using LDA. When the signals are classified

Table 14
Five-fold training and testing performance of the proposed MLP classifier using combined Microstates (MS) and Granger Causality (GC) features.

Fold	Accuracy	Precision	Recall	F1-Score	AUC	Loss
Training Performance						
1	0.9850	0.9895	0.9805	0.9850	0.9996	0.0150
2	0.9583	0.9548	0.9622	0.9585	0.9860	0.0417
3	0.9831	0.9882	0.9779	0.9830	0.9990	0.0169
4	0.9844	0.9819	0.9870	0.9844	0.9980	0.0156
5	0.9902	0.9896	0.9909	0.9902	0.9989	0.0098
Mean ± SD	**0.9808 ± 0.0125**	**0.9806 ± 0.0137**	**0.9793 ± 0.0109**	**0.9803 ± 0.0122**	**0.9963 ± 0.0062**	**0.0198 ± 0.0121**
Testing Performance						
1	0.7917	0.7414	0.8958	0.8113	0.8494	0.2083
2	0.8307	0.8432	0.8125	0.8276	0.8643	0.1693
3	0.6771	0.6828	0.6615	0.6720	0.7486	0.3229
4	0.7995	0.8142	0.7760	0.7947	0.8703	0.2005
5	0.8464	0.8556	0.8333	0.8443	0.8747	0.1536
Mean ± SD	**0.7891 ± 0.0614**	**0.7874 ± 0.0545**	**0.7958 ± 0.0849**	**0.7899 ± 0.0671**	**0.8419 ± 0.0480**	**0.2109 ± 0.0595**

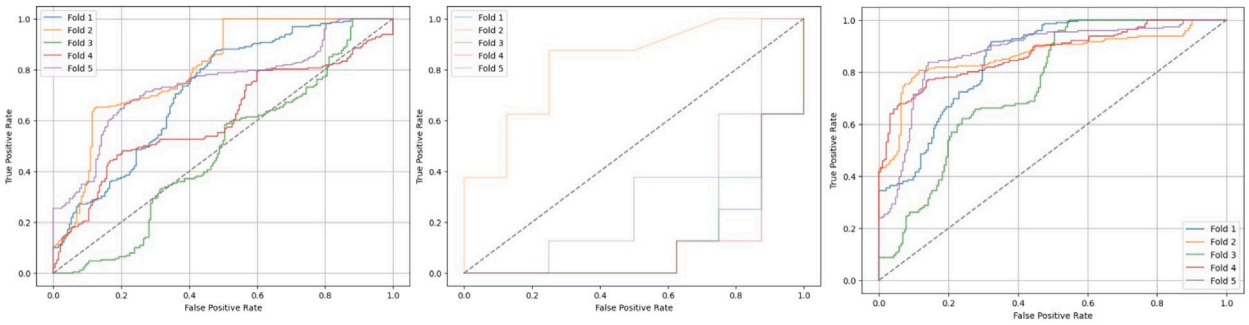

Fig. 20. ROC curves for group 5-fold based validation for MS and GC fusion. LDA (left), SVM (center), MLP (right).

Table 15
Group 5-fold based training and testing performance of the proposed SVM classifier using combined Transfer Entropy and Microstates features.

Fold	Accuracy	Precision	Recall	F1-Score	AUC	Loss
Training Performance						
1	0.9564	0.9511	0.9622	0.9566	0.9922	0.0436
2	0.9668	0.9723	0.9609	0.9666	0.9962	0.0332
3	0.9772	0.9754	0.9792	0.9773	0.9970	0.0228
4	0.8210	0.8077	0.8424	0.8247	0.8991	0.1790
5	0.7760	0.7650	0.7969	0.7806	0.8490	0.2240
Mean ± SD	**0.8995 ± 0.0831**	**0.8949 ± 0.0797**	**0.9085 ± 0.0757**	**0.9019 ± 0.0780**	**0.9265 ± 0.0633**	**0.1005 ± 0.0845**
Testing Performance						
1	0.7396	0.7674	0.6875	0.7253	0.7678	0.2604
2	0.4714	0.4796	0.6719	0.5597	0.4523	0.5286
3	0.5260	0.5410	0.3438	0.4204	0.5930	0.4740
4	0.6094	0.5778	0.8125	0.6753	0.6832	0.3906
5	0.5677	0.5448	0.8229	0.6556	0.6107	0.4323
Mean ± SD	**0.5824 ± 0.0951**	**0.5821 ± 0.1070**	**0.6673 ± 0.1964**	**0.6078 ± 0.1074**	**0.6114 ± 0.1160**	**0.4152 ± 0.0964**

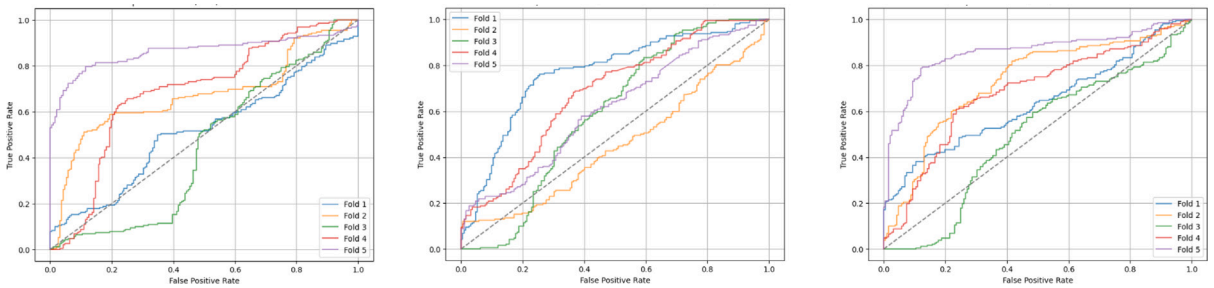

Fig. 21. ROC curves for group 5-fold based validation for Transfer Entropy and Microstates fusion, LDA (left), SVM (center), MLP (right).

Table 16
Group 5-fold based training and testing performance of the proposed MLP classifier using combined Transfer Entropy and Microstates features.

Training Performance						
Fold	Accuracy	Precision	Recall	F1-Score	AUC	Loss
1	0.6302	0.6302	0.6302	0.6302	0.6684	0.3698
2	0.7500	0.8750	0.5833	0.7000	0.8874	0.2500
3	0.5964	0.5768	0.7240	0.6420	0.5596	0.4036
4	0.7318	0.7486	0.6979	0.7224	0.7897	0.2682
5	0.8750	0.9000	0.8438	0.8710	0.9706	0.1250
Mean ± SD	**0.7167 ± 0.0973**	**0.7461 ± 0.1176**	**0.6956 ± 0.0973**	**0.7133 ± 0.0942**	**0.7759 ± 0.1545**	**0.2633 ± 0.0963**
Testing Performance						
1	0.5625	0.5583	0.5990	0.5779	0.6341	0.4375
2	0.5677	0.7708	0.1927	0.3083	0.7295	0.4323
3	0.5182	0.5131	0.7135	0.5970	0.4942	0.4818
4	0.6589	0.6432	0.7135	0.6765	0.6826	0.3411
5	0.7917	0.8784	0.6771	0.7647	0.8582	0.2083
Mean ± SD	**0.6190 ± 0.0941**	**0.6727 ± 0.1576**	**0.5799 ± 0.1963**	**0.5849 ± 0.1857**	**0.6793 ± 0.1475**	**0.3802 ± 0.0967**

Table 17
Group 5-Fold based training and testing performance of the proposed LDA classifier using combined Transfer Entropy (TE) and Microstates (MS) features.

Training Performance						
Fold	Accuracy	Precision	Recall	F1-Score	AUC	Loss
1	0.8053	0.8106	0.7969	0.8037	0.8692	0.1947
2	0.7943	0.8046	0.7773	0.7907	0.8306	0.2057
3	0.8542	0.8542	0.8542	0.8542	0.9152	0.1458
4	0.7643	0.7804	0.7357	0.7574	0.8522	0.2357
5	0.7819	0.8080	0.7396	0.7723	0.8557	0.2181
Mean ± SD	**0.8008 ± 0.0345**	**0.8111 ± 0.0310**	**0.7807 ± 0.0486**	**0.7957 ± 0.0350**	**0.8642 ± 0.0324**	**0.2000 ± 0.0338**
Testing Performance						
1	0.4948	0.4956	0.5833	0.5359	0.5158	0.5052
2	0.6797	0.7170	0.5938	0.6496	0.6712	0.3203
3	0.4922	0.4935	0.5885	0.5368	0.4462	0.5078
4	0.6328	0.6114	0.7292	0.6651	0.6866	0.3672
5	0.8333	0.8810	0.7708	0.8222	0.8629	0.1667
Mean ± SD	**0.6266 ± 0.1360**	**0.6397 ± 0.1607**	**0.5931 ± 0.0651**	**0.6419 ± 0.1182**	**0.6369 ± 0.1423**	**0.3734 ± 0.1300**

using individual features, the accuracy and other parameters give low performance, indicating that individual features are not sufficient to capture the discriminative patterns.

The attention mechanism sensitively captured the information from each modality by adaptively weighting the contribution based on task relevancy. This dynamic weighting of features diminishes the dimensional imbalance and noise reduction which is present in standalone feature sets. From the pattern observed from individual, partial fusion and full fusion of features, it is evaluated that no single type of feature is sufficient for capturing the dense multifaceted nature of neural dynamics in mental stress activity. Instead, the fusion of potential and diverse feature sets integrates the diverse underlying information, particularly in cases where both linear and non-linear information transfer is crucial. This technique further highlights the importance of combining connectivity features in neurophysiological analysis.

Discussion

The results are presented in Tables 6–8 illustrate the importance of feature-level fusion of multiple EEG modalities in the task of mental stress classification. The evaluation parameters show low performance of all three sets of features when used for classification individually. For instance, the accuracy of the fused feature set improved by 49.76%, 46.47% and 38.92% as compared to the individual feature set extracted from Granger Causality using SVM and LDA. Whereas with MLP, a slight decrease in performance of about 3.98% is observed.

Similarly, the attention-based fused feature set shows an improvement of 55.87%, +82.53%, 60.99% and 86.29%, 41.19%, 4.07% when compared with individual results obtained from Microstate-based and Transfer Entropy classification using SVM, LDA and MLP, respectively. It is observed that for MLP, the TE features outperform the full-fusion results.

The same trend was observed when the model fusion results were compared with the binary fusion of features. For example, the binary fusion of Granger Causality and Transfer Entropy provided about 0.22%, 54.91% and 18.66% improvement in the classification results compared with their full-fusion performance of both feature sets, respectively for SVM, LDA and MLP.

For SVM, the fully fuse model showed about 36.39% improved as compared with Granger Causality+ Microstates and about 53.90% and 6.03% improvement for LDA and MLP. Combining Microstates and Granger Causality gives a significant improvement in accuracy. Both features are robust in a way that they provide complementary mechanisms explained due to distinct interaction models. Granger Causality and Microstates showed complementary fusion. Granger Causality captured linear causality, and MS encodes the macro-level spatial organization. In this way, both of these features captured local and global brain responses while under stress. Similarly, for Microstates and Transfer Entropy, SVM achieved about 63.93%, LDA about 57.85% and MLP about 35.54% improvement.

Transfer entropy elevates the nonlinear information flow, i.e. under the stress condition, the frontal(including amygdala, hypothalamus) regions of the brain are activated. These regions send strong yet nonlinear energy bursts, indicating the high activity emerging in the prefrontal cortex. The non-linearity in the pre-frontal cortex is due to sudden response to attention and memory circuits (Rasheed et al., 2021). Transfer Entropy captures information transfer from the limbic and emotional areas into the prefrontal cortex (Rasheed et al., 2021). The classification result of about 70.05% (Table 7), 87.03% (Table 8)

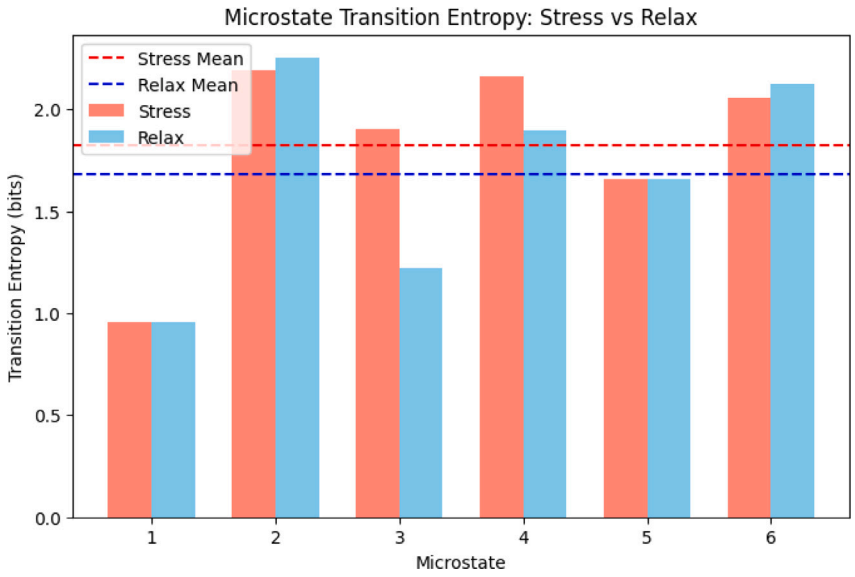

Fig. 22. Microstate transition entropy for stress and relax state.

and 51.25% (Table 6) showed that Transfer Entropy can capture the high information flow during stress conditions.

Granger Causality represents the directed linear influence of how one part of the brain regions statistically influences the other regions of the brain. As the activity in the pre-frontal cortex increases, showing the increase in attention and working memory, the shorter windowing mechanism reduces the directionality and leads to loss of control when there is reduced cognitive stability. In this way, the windowed Granger Causality methods show when, i.e. in which window and how fast the directions of activities change in that window (Yi et al., 2022).

Microstates are quasi-stable configurations of global brain activation that last roughly 100 ms. Under stress, the probability and speed of transitioning from one state to another increase, which makes the Microstates more unstable. This means that when under stress, the Microstate duration decreases and entropy increases. By entropy mean the measure of unpredictability of the next state. Unlike in the resting state, the Microstate patterns are not random. Fig. 22 represents the Microstate transition entropy for both stress and relax states. Higher entropy of stress (1.82) represents more unpredictability as compared to resting-state entropy (1.68). This indicates the rapid cognitive process during stressful conditions. The decrease in Microstate duration and increase in switching indicate the vigilance and less stable activity (Khanna et al., 2015).

Limitations

Despite these promising results, the proposed methodology has some shortcomings. Microstates are sensitive to transient changes in the brain. The extracted Microstate set is highly subject-specific and may not be generalizable to cross-subject variations. As mentioned in Khanna et al. (2015), the generalization of Microstates for study-task-based signals is still underdeveloped and requires a large cohort of standardized Microstates, tested against a test set, to ensure their reliability, thus enabling their use for cross-subject evaluation.

Interpolation across individual feature sets is essential for standardizing all features and ensuring consistency for the attention fusion model (Chiarion et al., 2023). However, it is important to note that interpolation can disrupt the temporal dynamics inherent in these features.

Features such as Transfer Entropy and Granger Causality matrices utilize windowing techniques, which help accommodate a degree of non-stationarity and temporal segmentation. Interpolation becomes necessary, especially for target feature sets that are computed over specific windows rather than the entire signal length. For example, transfer entropy is calculated using windows to capture non-linear relationships, while Microstates are evaluated over the full duration of the signal to represent global networks. Interpolation aids in smoothing out abrupt transitions caused by stress and cognitive switching. To enhance the robustness of the results, one could consider replacing conventional interpolation with alternative techniques, such as adaptive window-based interpolation.

Future works

The EEG-based multi-model fusion method provided profound results; however, it still needs further improvement and development. For instance, MS, GC and TE provided a first step for fusion; however, the set of modalities which are fused can be extended to other distinct feature-sets such as time-domain nd frequency-domain features. In this context, the following features could be integrated to enhance the functionality and usability:

- Deep-learning architectures can be used to model non-linear and spatial dependencies among Transfer Entropy, Microstates and Granger Causality. The deep learning models are better at capturing underlying inter-dependencies. Also, the attention-based fusion technique can be improved by using a transformer-based encoder for adaptive temporal weighting.
- Thought for static methods like Granger Causality and Transfer Entropy, windowing is used to preserve the time-related information, the dynamic trends can be improved by exploring dynamic Functional and Effective connectivity methods.
- The proposed framework is developed with the students as their target audience, who often feel stress due to exams and mental workload. However, this framework can be extended to validate further on other types of stress paradigms other than mental arithmetic stress, such as the Stroop test, social stress test, etc.
- To improve its real-world applicability, the fused set of features can be extended to other peripheral physiological signals (Chen et al., 2022) such as heart rate variability and Galvanic skin response, etc.

Conclusion

In this work, a new multi-feature-based neuromarker for accurate and effective stress classification for students based on EEG signals is proposed. By fusing three important EEG features, i.e. temporal microstates features, non-linear connectivity matrix, such as transfer

entropy and linear connectivity matrix Granger causality, which are combined using an attention fusion model. This fused set of features provided the classification results of 98% accuracy when classified using Group 5-fold Linear Discriminant Analysis. This work is presented to be the first work to combine Microstates, Transfer Entropy and Granger Causality for stress-based signals. Moreover, microstate analysis done on stress-based signal provided a new set of 6 distinct microstates which effectively captured stress-based dynamics. The fusion results were evaluated on the SAM40 dataset for mental arithmetic-based stress and relax signals. The proposed mode is compared with classification results of individual features as well as the binary fusion of the same features. This work not only provided a reliable biomarker for stress classification, rather it is also based on multiple modalities, each of which presents a distinct perspective of stress dynamics.

Funding

This work was supported by the European University of Atlantic.

Declaration of competing interest

The authors declare that they have no known competing financial interests or personal relationships that could have appeared to influence the work reported in this paper.

Availability of data and materials

The dataset used in this study can be requested from the corresponding author.

References

Akhand, M. A. H., Maria, M. A., Kamal, M. A. S., & Murase, K. (2023). Improved EEG-based emotion recognition through information enhancement in connectivity feature map. *Scientific Reports*, *13*(1), 13804.

Aloufi, M. A. (2021). Reducing stress, anxiety and depression in undergraduate nursing students: Systematic review. *Nurse Education Today*, *102*.

Alves, L. M., Côco, K. F., de Souza, M. L., & Ciarelli, P. M. (2022). Contextual microstates: an approach based on word embedding of microstates sequence to identify ADHD patients. *Research on Biomedical Engineering*

Arsalan, A., Majid, M., Butt, A. R., & Anwar, S. M. (2019). Classification of perceived mental stress using a commercially available EEG headband. *IEEE Journal of Biomedical and Health Informatics*, *23*(6), 2257–2264.

Asha, S. A., Sudalaimani, C., Devanand, P., Alexander, G., Lathikakumari, A. M., Thomas, S. V., & Ramshekhar, N. M. (2024). Analysis of EEG microstates as biomarkers in neuropsychological processes - review. *Computers in Biology and Medicind*, *173*, Article 108266.

Bahador, N., Jokelainen, J., Mustola, S., & Kortelainen, J. (2021). Multimodal spatio-temporal-spectral fusion for deep learning applications in physiological time series processing: A case study in monitoring the depth of anesthesia. *Information Fusion*, *73*, 125–143.

Bakare, S., Kuge, S., Sugandhi, S., Warad, S., & Panguddi, V. (2024). Detection of mental stress using EEG signals - alpha, beta, theta, and Gamma bands. In *2024 5th international conference for emerging technology*. IEEE.

Barnett, L., & Seth, A. K. (2014). The MVGC multivariate Granger causality toolbox: a new approach to Granger-causal inference. *Journal of Neuroscience Methods*, *223*, 50–68.

Bastos, A. M., & Schoffelen, J.-M. (2015). A tutorial review of functional connectivity analysis methods and their interpretational pitfalls. *Frontiers in System Neuroscience*, *9*, 175.

Bhatnagar, S., Khandelwal, S., Jain, S., & Vyawahare, H. (2023). A deep learning approach for assessing stress levels in patients using electroencephalogram signals. *Decision Analytics Journal*, *7*, Article 100211.

Bolton, M. L., Biltekoff, E., & Humphrey, L. (2023). The mathematical meaninglessness of the NASA task load index: A level of measurement analysis. *IEEE Transactions on Human-Machine Systems*, *53*(3), 590–599.

Botvinik-Nezer, R., & Wager, T. D. (2023). Reproducibility in neuroimaging analysis: Challenges and solutions. *Bioliogical Psychiatry: Cognitive Neuroscience and Neuroimaging*, *8*(8), 780–788.

Bouchrika, I. (2024). 50 current student stress statistics: 2024 data, analysis & predictions. *Education*.

Cai, H., Qu, Z., Li, Z., Zhang, Y., Hu, X., & Hu, B. (2020). Feature-level fusion approaches based on multimodal EEG data for depression recognition. *Information Fusion*, *59*, 127–138.

Cao, J., Zhao, Y., Shan, X., Wei, H.-L., Guo, Y., Chen, L., Erkoyuncu, J. A., & Sarrigiannis, P. G. (2022). Brain functional and effective connectivity based on electroencephalography recordings: A review. *Hum. Brain Mapp.*, *43*(2), 860–879.

Chen, J., Hu, B., Xu, L., Moore, P., & Su, Y. (2015). Feature-level fusion of multimodal physiological signals for emotion recognition. In *2015 IEEE international conference on bioinformatics and biomedicine* (pp. 395–399).

Chen, J., Liu, Y., Xue, W., Hu, K., & Lin, W. (2022). Multimodal EEG emotion recognition based on the attention recurrent graph convolutional network. *Information (Basel)*, *13*(11), 550.

Cheng, Q., Yang, W., Liu, K., Zhao, W., Wu, L., Lei, L., Dong, T., Hou, N., Yang, F., Qu, Y., & Yang, Y. (2019). Increased sample entropy in EEGs during the functional rehabilitation of an injured brain. *Entropy (Basel)*, *21*(7), 698.

Chiarion, G., Sparacino, L., Antonacci, Y., Faes, L., & Mesin, L. (2023). Connectivity analysis in EEG data: A tutorial review of the state of the art and emerging trends. *Bioengineering (Basel)*, *10*(3), 372.

Duan, J., Xiong, J., Li, Y., & Ding, W. (2024). Deep learning based multimodal biomedical data fusion: An overview and comparative review. *Information Fusion*, *112*(102536), Article 102536.

Gao, Y., Wang, X., Potter, T., Zhang, J., & Zhang, Y. (2020). Single-trial EEG emotion recognition using granger Causality/Transfer entropy analysis. *Journal of Neuroscience Methods*, *346*(108904), Article 108904.

Ghosh, R., Deb, N., Sengupta, K., Phukan, A., Choudhury, N., Kashyap, S., Phadikar, S., Saha, R., Das, P., Sinha, N., & Dutta, P. (2022). SAM 40: Dataset of 40 subject EEG recordings to monitor the induced-stress while performing stroop color-word test, arithmetic task, and mirror image recognition task. *Data in Brief*, *40*, Article 107772.

Goenka, U., Patil, P., Gosalia, K., & Jagetia, A. (2022). Classification of electroencephalograms during mathematical calculations using deep learning. In *2022 IEEE 23rd international conference on information reuse and integration for data science* (pp. 12–17).

Guo, Z., McClelland, V. M., Simeone, O., Mills, K. R., & Cvetkovic, Z. (2022). Multiscale wavelet transfer entropy with application to corticomuscular coupling analysis. *IEEE Transactions on Biomedical Engineering*, *69*(2), 771–782.

Hag, A., Handayani, D., Pillai, T., Mantoro, T., Kit, M. H., & Al-Shargie, F. (2021). EEG mental stress assessment using hybrid multi-domain feature sets of functional connectivity network and time-frequency features. *Sensors (Basel)*, *21*(18), 6300.

Han, Q., Li, T., Li, W., Zhao, J., Kuang, Z., & Shi, L. (2025). A cognitive impairment disorders recognition framework based on EEG microstate. In *Proceedings of the 4th international conference on computer, artificial intelligence and control engineering* (pp. 96–101). New York, NY, USA: ACM.

Hasan, M. J., & Kim, J.-M. (2019). A hybrid feature pool-based emotional stress state detection algorithm using EEG signals. *Brain Sciences*, *9*(12), 376.

Haydock, D., Kadir, S., Leech, R., Nehaniv, C. L., & Antonova, E. (2025). EEG microstate syntax analysis: A review of methodological challenges and advances. *Neuroimage*, *309*(121090), Article 121090.

Hu, L., & Zhang, Z. (Eds.), (2019). *EEG signal processing and feature extraction* (2019 ed.). Singapore, Singapore: Springer.

Huckins, J. F., daSilva, A. W., Wang, W., Hedlund, E., Rogers, C., Nepal, S. K., Wu, J., Obuchi, M., Murphy, E. I., Meyer, M. L., Wagner, D. D., Holtzheimer, P. E., & Campbell, A. T. (2020). Mental health and behavior of college students during the early phases of the COVID-19 pandemic: Longitudinal smartphone and ecological momentary assessment study. *Journal of Medical Internet Research*, *22*(6), Article e20185.

Javaid, H., Nouman, M., Cheaha, D., Kumarnsit, E., & Chatpun, S. (2024). Complexity measures reveal age-dependent changes in electroencephalogram during working memory task. *Behavioral Brain Research*, *470*(115070), Article 115070.

Khanna, A., Pascual-Leone, A., Michel, C. M., & Farzan, F. (2015). Microstates in resting-state EEG: current status and future directions. *Neuroscience & Biobehavioral Reviews*, *49*, 105–113.

Kim, K., Duc, N. T., Choi, M., & Lee, B. (2021). EEG microstate features according to performance on a mental arithmetic task. *Scientific Reports*, *11*(1), 343.

Kleinert, T., Koenig, T., Nash, K., & Wascher, E. (2024). On the reliability of the EEG microstate approach. *Brain Topography*, *37*(2), 271–286.

Koenig, T., Diezig, S., Kalburgi, S. N., Antonova, E., Artoni, F., Brechet, L., Britz, J., Croce, P., Custo, A., Damborská, A., Deolindo, C., Heinrichs, M., Kleinert, T., Liang, Z., Murphy, M. M., Nash, K., Nehaniv, C., Schiller, B., Smailovic, U., ... Michel, C. M. (2024). EEG-meta-microstates: Towards a more objective use of resting-state EEG microstate findings across studies. *Brain Topography*, *37*(2), 218–231.

Li, J., Li, N., Shao, X., Chen, J., Hao, Y., Li, X., & Hu, B. (2023). Altered brain dynamics and their ability for major depression detection using EEG microstates analysis. *IEEE Transactions on Affective Computing*, *14*(3), 2116–2126.

Liu, S., Gao, P., Li, Y., Fu, W., & Ding, W. (2023). Multi-modal fusion network with complementarity and importance for emotion recognition. *Information Sciences*, *619*, 679–694.

Liu, Q., Jia, S., Tu, N., Zhao, T., Lyu, Q., Liu, Y., Song, X., Wang, S., Zhang, W., Xiong, F., Zhang, H., Guo, Y., & Wang, G. (2024). Open access EEG dataset of repeated measurements from a single subject for microstate analysis. *Scientific Data*, *11*(1).

Liu, Z., Si, L., Xu, W., Zhang, K., Wang, Q., Chen, B., & Wang, G. (2022). Characteristics of EEG microstate sequences during propofol-induced alterations of brain consciousness states. *IEEE Transactions on Neural Systems and Rehabilitation Engineering*, *30*, 1631–1641.

Ma, X., Chen, W., Pei, Z., Zhang, Y., & Chen, J. (2024). Attention-based convolutional neural network with multi-modal temporal information fusion for motor imagery EEG decoding. *Computers in Biology and Medicine*, *175*(108504), Article 108504.

Malviya, L., & Mal, S. (2022). A novel technique for stress detection from EEG signal using hybrid deep learning model. *Neural Computing and Applications*, *34*(22), 19819–19830.

Michel, C. M., & Koenig, T. (2018). EEG microstates as a tool for studying the temporal dynamics of whole-brain neuronal networks: a review. *NeuroImage*, *180*, 577–593.

Pascual-Marqui, R. D., Michel, C. M., & Lehmann, D. (1995). Segmentation of brain electrical activity into microstates: model estimation and validation. *IEEE Transactions on Biomedical Engineering*, *42*(7), 658–665.

Pichandi, S., Balasubramanian, G., Chakrapani, V., & Manoharan, J. S. (2025). Optimized deep learning models for stress-based stroke prediction from EEG signals. *Discover Applied Sciences*, *7*(6).

Pillalamarri, R., & Shanmugam, U. (2025). A review on EEG-based multimodal learning for emotion recognition. *Artificial Intelligence Review*, *58*(5).

Placek, M. M., Beqiri, E., Czosnyka, M., & Smielewski, P. (2022). Technical considerations on the use of granger causality in neuromonitoring. *Brain Multiphysics*, *3*, Article 100044.

Qiu, J.-L., Liu, W., & Lu, B.-L. (2018). Multi-view emotion recognition using deep canonical correlation analysis. In *Lecture notes in computer science*, *Neural information processing* (pp. 221–231). Cham: Springer International Publishing.

Radman, M., Moradi, M., Chaibakhsh, A., Kordestani, M., & Saif, M. (2021). Multi-feature fusion approach for epileptic seizure detection from EEG signals. *IEEE Sensors Journal*, *21*(3), 3533–3543.

Rajendran, V., Jayalalitha, S., & Adalarasu, K. (2022). EEG based evaluation of examination stress and test anxiety among college students. *IRBM*, *43*(5), 349–361.

Ramakrishna, J. S., Sinha, N., & Ramasangu, H. (2021). Classification of human emotions using EEG-based causal connectivity patterns. In *2021 IEEE conference on computational intelligence in bioinformatics and computational biology*. IEEE.

Rasheed, K., Qayyum, A., Qadir, J., Sivathamboo, S., Kwan, P., Kuhlmann, L., O'Brien, T., & Razi, A. (2021). Machine learning for predicting epileptic seizures using EEG signals: A review. *IEEE Reviews in Biomedical Engineering*, *14*, 139–155.

Rashmi, C. R., & Shantala, C. P. (2023). BCI-AMSH: A MATLAB based open-source brain computer interface assistive application for mental stress healing. *E-Prime - Advances in Electrical Engineering, Electronics and Energy*, *6*, Article 100323.

Restrepo, J. F., Mateos, D. M., & López, J. M. D. (2023). A transfer entropy-based methodology to analyze information flow under eyes-open and eyes-closed conditions with a clinical perspective. *Biomedical Signal Processing and Control*, *86*(105181), Article 105181.

Sadeghijam, M., Talebian, S., Mohsen, S., Akbari, M., & Pourbakht, A. (2021). Shannon entropy measures for EEG signals in tinnitus. *Neuroscience Letters*, *762*(136153), Article 136153.

Shamsi, F., Haddad, A., & Najafizadeh, L. (2021). Early classification of motor tasks using dynamic functional connectivity graphs from EEG. *Journal of Neural Engineering*, *18*(1), Article 016015.

Si, X., Huang, H., Yu, J., & Ming, D. (2024). EEG microstates and fNIRS metrics reveal the spatiotemporal joint neural processing features of human emotions. *IEEE Transactions on Affective Computing*, *15*(4), 2128–2138.

Sohrabpour, A., Ye, S., Worrell, G. A., Zhang, W., & He, B. (2016). Noninvasive electromagnetic source imaging and granger causality analysis: An electrophysiological connectome (eConnectome) approach. *IEEE Transactions on Biomedical Engineering*, *63*(12), 2474–2487.

Swapnil, S. S., Nuhi-Alamin, M., Rahman, K. M., Sarkar, A. K., & Siam, M. Z. H. (2024). An ensemble approach to classify mental stress using EEG based time-frequency and non-linear features. In *2024 3rd international conference on advancement in electrical and electronic engineering* (pp. 1–6).

Tarailis, P., Koenig, T., Michel, C. M., & Griškova-Bulanova, I. (2024). The functional aspects of resting EEG microstates: A systematic review. *Brain Topography*, *37*(2), 181–217.

Terpou, B. A., Shaw, S. B., Théberge, J., Férat, V., Michel, C. M., McKinnon, M. C., Lanius, R. A., & Ros, T. (2022). Spectral decomposition of EEG microstates in post-traumatic stress disorder. *NeuroImage: Clinical*, *35*(103135), Article 103135.

Vignaud, P. (2023). Can a single session of noninvasive brain stimulation applied over the prefrontal cortex prevent stress-induced cortisol release? *Progress in Neuro-Psychopharmacology and Biological Psychiatry*, *121*.

Xiong, X., Ji, X., Yi, S., Wang, C., Liu, R., & He, J. (2025). Motor imagery EEG microstates are influenced by alpha power. *Computer Methods in Biomechanics and Biomedical Engineering*, 1–16.

Yang, J., Yin, Y., Zhang, Z., Long, J., Dong, J., Zhang, Y., Xu, Z., Li, L., Liu, J., & Yuan, Y. (2018). Predictive brain networks for major depression in a semi-multimodal fusion hierarchical feature reduction framework. *Neuroscience Letters*, *665*, 163–169.

Yedukondalu, J., Sharma, D., & Sharma, L. D. (2024). Subject-wise cognitive load detection using time–frequency EEG and bi-LSTM. *Arabian Journal for Science and Engineering*, *49*(3), 4445–4457.

Yi, C., Qiu, Y., Chen, W., Chen, C., Wang, Y., Li, P., Yang, L., Zhang, X., Jiang, L., Yao, D., Li, F., & Xu, P. (2022). Constructing time-varying directed EEG network by multivariate nonparametric dynamical granger causality. *IEEE Transactions on Neural Systems and Rehabilitation Engineering*, *30*, 1412–1421.

Yi, C., Zhang, J., Weng, Z., Chen, W., Yao, D., Li, F., Cao, Z., Li, P., & Xu, P. (2024). Nonparametric dynamic granger causality based on multi-space spectrum fusion for time-varying directed brain network construction. *IEEE Journal of Biomedical and Health Informatics*, 1–10.

Zhang, B., Wei, D., Yan, G., Lei, T., Cai, H., & Yang, Z. (2022). Feature-level fusion based on spatial-temporal of pervasive EEG for depression recognition. *Computer Methods and Programs in Biomedicine*, *226*(107113), Article 107113.

Zhang, Y., Yan, G., Chang, W., Huang, W., & Yuan, Y. (2023). EEG-based multi-frequency band functional connectivity analysis and the application of spatio-temporal features in emotion recognition. *Biomedical Signal Processing and Control*, *79*(104157), Article 104157.

Zhang, J., Yin, Z., Chen, P., & Nichele, S. (2020). Emotion recognition using multi-modal data and machine learning techniques: A tutorial and review. *Information Fusion*, *59*, 103–126.

Zhu, S., Yi, W., Wang, S., Wang, Q., Bai, D., Liu, W., & Wang, J. (2025). Phase slope transfer entropy analysis of EEG in patients with Parkinson's disease. *Biomedical Signal Processing and Control*, *100*(107043), Article 107043.